Nonperturbative feats in the physics of correlated antiferromagnets

M. Reitner [1,*] L. Del Re [2,3] M. Capone [4,5] and A. Toschi [1]

[1]*Institute of Solid State Physics, TU Wien, 1040 Vienna, Austria*

[2]*Institut für Theoretische Physik und Astrophysik and Würzburg-Dresden Cluster of Excellence ct.qmat, Universität Würzburg, 97074 Würzburg, Germany*

[3]*Max-Planck-Institut für Festkörperforschung, Heisenbergstraße 1, 70569 Stuttgart, Germany*

[4]*International School for Advanced Studies (SISSA), Via Bonomea 265, 34136 Trieste, Italy*

[5]*CNR-IOM, Istituto Officina dei Materiali, Consiglio Nazionale delle Ricerche, Via Bonomea 265, 34136 Trieste, Italy*

(Received 25 November 2024; accepted 17 August 2025; published 18 September 2025)

In the last decades, multifaceted manifestations of the breakdown of the self-consistent perturbation theory have been identified for the many-electron problem. Yet, the investigations have been so far mostly limited to paramagnetic states, where symmetry breaking is not allowed. Here, we extend the analysis to the spontaneously symmetry-broken antiferromagnetic (AF) phase of the repulsive Hubbard model. To this aim, we calculated two-particle quantities using dynamical mean-field theory for the AF-ordered Hubbard model and studied the possible occurrence of divergences of the irreducible vertex functions in the charge and spin sectors. Our calculations pinpoint the divergences in the AF phase diagram, showing that while the onset of AF order mitigates the breakdown of the perturbation expansion, it does not fully prevent it. Moreover, we have been able to link the changes in the dynamical structure of the corresponding generalized susceptibilities to the physical crossover from a weak-coupling (Slater) to a strong-coupling (Heisenberg) antiferromagnet, which takes place as the interaction strength is gradually increased. Finally, we discuss possible physical consequences of the irreducible vertex divergences in triggering phase-separation instabilities within the AF phase and elaborate on the implications of our findings for two-dimensional systems, where the onset of a long-range AF order is prevented by the Mermin-Wagner theorem.

DOI: 10.1103/ympr-9m73

I. INTRODUCTION

Several of the most fascinating phenomena in condensed matter theory, such as unconventional high-temperature superconductivity, quantum criticality [1–4], or the appearance of nontrivial features in spectroscopic experiments (pseudogap [5–7], waterfalls [8], and hourglasses, to cite a few), occur in materials in which the screening of the on-site electron-electron interaction works rather poorly. As a result, the quantum field theoretical description of the underlying many-electron physics needs to be pursued in parameter regimes where the validity of the many-body perturbation expansion is not guaranteed *a priori*. This arguably explains the efforts made in the last decade by several research groups to investigate all multifaceted manifestations of the breakdown of the self-consistent perturbation theory, on both a formal [9–19] and a physical [20–25] level.

In a nutshell, we recall that the major manifestations of such breakdown are the misleading convergence of the self-consistent (bold) perturbation expansion [10,11,15,16] in broad parameter regimes of the many-electron problem, as well as the associated [13] divergences of the irreducible two-particle vertex functions [9,12,17,19,26,27]. While the relevance of these nonperturbative features for algorithmic schemes based on resummations of bold Feynman diagrams or on parquet equations is immediately evident, recently a clear link between such formal aspects of the many-electron theory and the underlying physical properties has been identified. In particular, the breakdown of the self-consistent perturbation expansion appears to be directly driven [21–24] by one of the major hallmarks of the correlated electron physics, i.e., the gradual formation of local magnetic moments and the *simultaneous* suppression of on-site charge fluctuations. Furthermore, under certain conditions, its occurrence can even reverse the sign of the effective electronic interaction at low energies, turning it into an attraction [20,28]. The latter has been shown to trigger phase-separation instabilities in (purely repulsive) electronic systems [18,20,25], and prospectively, it can lead to significant renormalization of the electron-phonon coupling [29,30] and/or of the electronic pairing [31–33] in the presence of strong correlations.

The investigation of these issues has been typically carried out, nonperturbatively, by means of analytical calculations [10,11,13,15,19,26] of simplified models and of numerically precise treatments [12,14,21,34] of single-impurity Anderson models and, above all, by solving, on the two-particle level

*Contact author: matthias.reitner@outlook.com

Published by the American Physical Society under the terms of the Creative Commons Attribution 4.0 International license. Further distribution of this work must maintain attribution to the author(s) and the published article's title, journal citation, and DOI.

[9,10,12,16,17,20,21,24–27], the Hubbard model via dynamical mean-field theory (DMFT) [35] or its cluster extensions [36].

Hitherto, however, all these studies[1] were performed in the paramagnetic (PM) phase, i.e., not allowing for any spontaneous breaking of the SU(2) symmetry *even* in situations where the low-temperature phase of the system considered is known to display a thermodynamically stable antiferromagnetic (AF) long-range ordering.

Indeed, despite the higher numerical effort of performing two-particle calculations in a lower-symmetry phase, an extension of the previous investigations to the AF-ordered regime would be important for several reasons.

On a fundamental level, the study of the breakdown of the bold perturbation expansion in the presence of a (thermodynamically stable) AF ordering could allow for a precise understanding of the competitive interplay between long-range order and electronic correlation, beyond the intriguing effects already observed at the one-particle level [37,38] that highlighted the crucial relevance of many-body effects beyond mean field in the AF phase.

On a more physical level, such a study could unveil whether the onset of long-range order can mitigate the breakdown of perturbation theory, following the intuition that the singularities of the theory can be weakened in the broken symmetry AF state. Further, our analysis could clarify the underlying relations between the breakdown of the perturbation theory and the different regimes of a correlated antiferromagnet, which typically evolves from a Slater AF at weak coupling (whose stabilization, driven by nesting on bipartite lattices, is associated with a potential energy gain) to a Heisenberg AF (whose stabilization, driven by the onset of coherence between preformed local moments, is associated with a kinetic energy gain). We notice that this evolution is not specific to the AF solution, but it is expected to be quite general. For instance, it is found also for the superconducting phase of the attractive Hubbard model, where it corresponds to the BCS-BEC crossover [39].

Finally, from an algorithmic perspective, the information that could be gained from these investigations might provide crucial hints for the future development and the applicability of bold diagrammatic resummation schemes and/or of diagrammatic extensions [40] of DMFT or two-particle self-consistent theory [41] in the SU(2)-broken-symmetry phases [42,43].

For these reasons, in this paper, we extend the previous studies of the manifestations of the perturbation theory breakdown to the AF-ordered phase. To this aim, we have systematically performed two-particle DMFT calculations in the low-temperature AF-ordered phase of the half filled Hubbard model. These calculations allow for a thorough investigation of possible divergences appearing in the irreducible vertex functions, as well as to study their relation with specific physical properties that characterize, respectively, the Slater and the Heisenberg AF regime. For a comparative analysis of the nonperturbative effects in the symmetry-broken phase with respect to approximation schemes, which rely on the self-consistent perturbation expansion, we integrate our DMFT study with corresponding calculations in conventional static mean-field theory and the random phase approximation (MF/RPA).

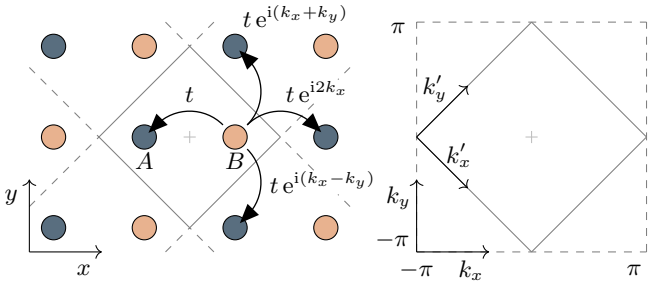


FIG. 1. Left: Bipartite Hubbard model on the square lattice. In the Fourier transform, the hopping parameters to the next neighbors acquire a phase factor depending on the distance of their unit cells (squares). Right: Reduced Brillouin zone of the bipartite model.

The paper is structured as follows: In Sec. II, we define the specific Hubbard model, as well as the necessary one- and two-particle quantities for our DMFT and MF/RPA calculations. Section III shows our DMFT results for the divergences of the irreducible vertex in the AF phase and investigates their appearance in connection to the different behavior of the local physical charge response in the Slater and Heisenberg AF. Section IV takes an eigenvalue perspective on the Bethe-Salpeter equation (BSE) in the AF phase and discusses possible consequences for phase-separation instabilities. Conclusion and outlook of the paper are presented in Secs. V and VI, respectively.

II. FORMALISM AND METHODS

A. Bipartite Hubbard model in mean-field and dynamical mean-field theory

We study a bipartite square lattice Hubbard model with nearest-neighbor hopping $t = 1/4$, whose Hamiltonian reads

$$H = \sum_{\mathbf{k}\sigma} (\hat{c}^\dagger_{A\mathbf{k}\sigma},\ \hat{c}^\dagger_{B\mathbf{k}\sigma}) \begin{pmatrix} -\mu & \varepsilon_{\mathbf{k}} \\ \varepsilon^*_{\mathbf{k}} & -\mu \end{pmatrix} \begin{pmatrix} \hat{c}_{A\mathbf{k}\sigma} \\ \hat{c}_{B\mathbf{k}\sigma} \end{pmatrix} + U \sum_{i\alpha} \hat{n}_{\alpha i\uparrow} \hat{n}_{\alpha i\downarrow}, \tag{1}$$

where μ is the chemical potential, U the Hubbard interaction, $\hat{n}_{\alpha i\sigma} = \hat{c}^\dagger_{\alpha i\sigma} \hat{c}_{\alpha i\sigma}$ the occupation of spin σ on site $\alpha = (A, B)$ in the ith unit cell, $\hat{c}^{(\dagger)}_{\alpha\mathbf{k}\sigma}$ the corresponding Fourier transform, and $\varepsilon_{\mathbf{k}} = -2t\, e^{ik_x}(\cos k_x + \cos k_y)$ the dispersion relation (see Fig. 1), where $\mathbf{k}$ runs over the reduced Brillouin

[1]We note here the partial exception of Ref. [19], where the SU(2) symmetry is explicitly broken by an external magnetic field in the basic case of a Hubbard atom.

zone (RBZ):[2] $k_x = k'_x + k'_y$ and $k_y = k'_y - k'_x$, with $k'_x, k'_y \in [(-\pi/2, -\pi/2), (\pi/2, \pi/2))$.

At particle-hole (ph) symmetry $\mu = U/2$, which corresponds to half filling $n = n_{\alpha\uparrow} + n_{\alpha\downarrow} = \langle \hat{n}_{\alpha\uparrow} + \hat{n}_{\alpha\downarrow} \rangle = 1$, and zero temperature, the model is expected to order antiferromagnetically with a nonzero staggered magnetization $m = m_A = n_{A\uparrow} - n_{A\downarrow} = -m_B$ on the two lattice sites. Without loss of generality, such magnetization (if present) can be oriented along the z axis, and the corresponding Dyson equation then reads

$$G_{k\sigma} = \begin{pmatrix} G^{AA}_{k\sigma} & G^{AB}_{k\sigma} \\ G^{BA}_{k\sigma} & G^{BB}_{k\sigma} \end{pmatrix} = \frac{1}{\zeta_{Ak\sigma}\zeta_{Bk\sigma} - |\varepsilon_{\mathbf{k}} + \Sigma_{ABk\sigma}|^2} \begin{pmatrix} \zeta_{Bk\sigma} & \varepsilon_{\mathbf{k}} + \Sigma_{ABk\sigma} \\ \varepsilon^*_{\mathbf{k}} + \Sigma^*_{ABk\sigma} & \zeta_{Ak\sigma} \end{pmatrix}, \tag{2}$$

where $\zeta_{\alpha k\sigma} = i\nu + \mu - \Sigma_{\alpha k\sigma}$, the fermionic Matsubara frequencies are defined as $\nu = (2n+1)\pi T$, with $n \in \mathbb{Z}$, and $\Sigma_{\alpha k\sigma}$ is the electronic self-energy on site α and $\Sigma_{ABk\sigma} = \Sigma^*_{BAk\sigma}$ between sites A and B, with $k = (\nu, \mathbf{k})$.

From the symmetry $(A, \sigma) \leftrightarrow (B, -\sigma)$ in the AF phase, it follows that $\zeta_{Bk\sigma} = \zeta_{Ak-\sigma}$. In the PM phase, when $\zeta_{\alpha k\sigma} = \zeta_{\alpha k-\sigma}$, diagonalizing the matrix $G_{k\sigma}$ returns two Green's functions

$$\mathcal{G}_{k\sigma\pm} = \frac{1}{\zeta_{k\sigma} \pm |\varepsilon_{\mathbf{k}} + \Sigma_{ABk\sigma}|} \tag{3}$$

associated with the two "bands" in the RBZ, corresponding to $\mathbf{k}$ and $\mathbf{k} + (\pi, \pi)$ of the full Brillouin zone (BZ).

In the course of the paper, we study the half filled Hubbard model within two self-consistent approximate methods, namely, (1) the perturbative conventional static MF/RPA approach and (2) the nonperturbative DMFT. By means of the latter, we directly extend the study of nonperturbative effects reported in recent literature [18,20,21,24,25] to the symmetry-broken phase. It is important to recall that, while being conserving approximations [44], both RPA and DMFT do not fulfill the Mermin-Wagner theorem, yielding an antiferromagnetic-ordered phase at finite temperatures in two dimensions. Our two-dimensional (2D) results are expected to be qualitatively similar to those of a three-dimensional (3D) Hubbard model, where an actual AF long-range order is expected also at finite temperature. Such an agreement could even turn quantitative if we scale the hopping in order to have the same variance of the noninteracting density of states in two and three dimensions.[3]

Due to such a fairly good equivalence, at the DMFT level, we decided to perform our calculations in two dimensions. This allows us to better match the recent literature developments [46,47], which restore the Mermin-Wagner theorem starting from a symmetry-broken (dynamical) mean-field solution, as well as to provide a reference for future nonperturbative studies of generalized two-particle susceptibilities and vertex functions of 2D systems beyond the local DMFT realm. We will elaborate on the plausible consequences of our results for the Hubbard model in two dimensions in Sec. VI.

In both methods, MF/RPA and DMFT, the self-energy only contributes on site $\Sigma_{ABk\sigma} = 0$ and $\Sigma_{\alpha k\sigma}$ becomes independent of $\mathbf{k}$: (1) in MF/RPA, $\Sigma_{\alpha k\sigma} \approx (U/2)(n - m_\alpha)$, and (2) in DMFT, $\Sigma_{\alpha k\sigma} \approx \Sigma_{\alpha\nu\sigma}$ [35]. For the latter, $\Sigma_{\alpha\nu\sigma}$ corresponds to the on-site self-energy calculated from an auxiliary Anderson impurity model (AIM), which in our case is solved using the continuous-time quantum Monte Carlo [48] w2dynamics [49] software package.

In the MF approximation (1), the self-consistency is achieved from iterated calculations of the static staggered magnetization [50]

$$m_\alpha = \frac{1}{V\beta} \sum_k \left(G^{\alpha\alpha}_{k\uparrow} - G^{\alpha\alpha}_{k\downarrow} \right) e^{i\nu 0^+}, \tag{4}$$

where $V = \mathfrak{V}/2$ is half of the volume $\mathfrak{V}$ and $\beta = 1/T$ the inverse temperature. However, in DMFT (2), the condition of self-consistency is attained from the calculation of the (frequency-dependent) local Green's function [35]

$$G^{\alpha\alpha}_{\nu\sigma} = \frac{1}{V} \sum_{\mathbf{k}} G^{\alpha\alpha}_{k\sigma} = \frac{1}{\zeta_{\alpha\nu\sigma} - \Delta_{\alpha\nu\sigma}}, \tag{5}$$

where $\Delta_{\alpha\nu\sigma}$ is the hybridization function of the AIM.

B. Generalized susceptibilities

Information about the physical response and fluctuations in charge and spin degrees of freedom of the model is encoded at the two-particle level in the generalized susceptibilities [40,51,52], defined as

$$\chi^{\alpha\alpha' kk'}_{q\sigma\sigma'} = \int d\tau_1 d\tau_2 d\tau_3 \, e^{-i\nu\tau_1} e^{i(\nu+\omega)\tau_2} e^{-i(\nu'+\omega)\tau_3} \times \left[\langle \mathcal{T} \hat{c}^\dagger_{\alpha\mathbf{k}\sigma}(\tau_1) \hat{c}_{\alpha\mathbf{k}+\mathbf{q}\sigma}(\tau_2) \hat{c}^\dagger_{\alpha'\mathbf{k}'+\mathbf{q}\sigma'}(\tau_3) \hat{c}_{\alpha'\mathbf{k}'\sigma'}(0) \rangle - \langle \mathcal{T} \hat{c}^\dagger_{\alpha\mathbf{k}\sigma}(\tau_1) \hat{c}_{\alpha\mathbf{k}+\mathbf{q}\sigma}(\tau_2) \rangle \langle \mathcal{T} \hat{c}^\dagger_{\alpha'\mathbf{k}'+\mathbf{q}\sigma'}(\tau_3) \hat{c}_{\alpha'\mathbf{k}'\sigma'}(0) \rangle \right], \tag{6}$$

where σ, σ' denote the spins on sites α, α' with fermionic $k = (\nu, \mathbf{k}), k' = (\nu', \mathbf{k}')$ and bosonic $q = (\omega, \mathbf{q})$ ($\omega = 2n\pi T$, $n \in \mathbb{Z}$) four-momenta, $\mathcal{T}$ denotes the imaginary time ordering operator, and $\langle \cdots \rangle = (1/Z)\mathrm{Tr}(e^{-\beta H} \cdots)$ is the thermal expectation value. To shorten the notation, we define the generalized susceptibilities corresponding to the momentum-dependent response of our square lattice system as

$$\boldsymbol{\chi}^{\alpha\alpha'}_{\mathbf{q}\sigma\sigma'}(\omega) \coloneqq \frac{1}{V^2} \sum_{\mathbf{k}\mathbf{k}'} \chi^{\alpha\alpha' kk'}_{q\sigma\sigma'}, \tag{7}$$

i.e., as matrices in the fermionic frequency space ν, ν'. Further, for quantities corresponding to the static/isothermal $\omega = 0$ response [53], we will omit the corresponding zero transfer frequency argument $\boldsymbol{\chi}^{\alpha\alpha'}_{\mathbf{q}\sigma\sigma'} \coloneqq \boldsymbol{\chi}^{\alpha\alpha'}_{\mathbf{q}\sigma\sigma'}(0)$. The local generalized susceptibilities $\boldsymbol{\chi}^{\alpha\alpha'}_{\sigma\sigma'}(\omega)$ (in MF/RPA) can then be obtained by

[2] We choose the basis of the bipartite lattice such that the dispersion remains periodic within the reduced Brillouin zone [45].

[3] For instance, this can be realized by taking $t = 1/4$ for a 2D square lattice (as done here) and $t = 1/(2\sqrt{6})$ for a 3D cubic lattice [35].

summing over all momenta $\mathbf{q}$:

$$\chi^{\alpha\alpha'}_{\sigma\sigma'}(\omega) = \frac{1}{V}\sum_{\mathbf{q}} \chi^{\alpha\alpha'}_{\mathbf{q}\sigma\sigma'}(\omega), \tag{8}$$

which in the limit of infinite lattice connectivity, where DMFT becomes rigorously exact [35,54], would also correspond to the on-site generalized susceptibilities $\chi_{\sigma\sigma'} = \chi^{AA}_{\sigma\sigma'} = \chi^{BB}_{-\sigma-\sigma'}$ and $\chi^{\alpha\alpha'}_{\sigma\sigma'} = \delta_{\alpha\alpha'}\chi^{\alpha\alpha}_{\sigma\sigma'}$ of the auxiliary AIM of the self-consistent DMFT solution. In the two-dimensional case considered here, where DMFT is an approximation, the generalized susceptibilities of the auxiliary AIM will be used for the calculations of the corresponding local quantities.

We also recall that, for noninteracting systems as well as when all two-particle scattering processes (i.e., the so-called vertex corrections) are neglected, the susceptibility expressions above reduce to the corresponding "bubble" terms, defined as

$$\chi^{\alpha\alpha'}_{0\mathbf{q}\sigma\sigma'}(\omega) = -\frac{\beta}{V}\sum_{\mathbf{k}} \delta_{\nu\nu'}\delta_{\sigma\sigma'} G^{\alpha\alpha'}_{k\sigma} G^{\alpha'\alpha}_{k+q\sigma}, \tag{9}$$

and, for the on-site counterpart, as

$$\chi_{0\sigma\sigma'}(\omega) = \frac{1}{V}\sum_{\mathbf{q}} \chi^{AA}_{0\mathbf{q}\sigma\sigma'}(\omega) = \frac{1}{V}\sum_{\mathbf{q}} \chi^{BB}_{0\mathbf{q}-\sigma-\sigma'}(\omega). \tag{10}$$

To obtain the local generalized susceptibilities in the usual charge (c) and spin (s) notation

$$\chi = \begin{pmatrix} \chi_s & \chi_{sc} \\ \chi_{cs} & \chi_c, \end{pmatrix}, \tag{11}$$

which is directly associated with the local density and magnetic linear response of the system, we use the following definitions (cf. also Ref. [42]):

$$\chi_s = \tfrac{1}{2}(\chi_{\uparrow\uparrow} + \chi_{\downarrow\downarrow} - \chi_{\uparrow\downarrow} - \chi_{\downarrow\uparrow}), \tag{12}$$

$$\chi_{sc} = \tfrac{1}{2}(\chi_{\uparrow\uparrow} - \chi_{\downarrow\downarrow} + \chi_{\uparrow\downarrow} - \chi_{\downarrow\uparrow}), \tag{13}$$

$$\chi_c = \tfrac{1}{2}(\chi_{\uparrow\uparrow} + \chi_{\downarrow\downarrow} + \chi_{\uparrow\downarrow} + \chi_{\downarrow\uparrow}), \tag{14}$$

$$\chi_{cs} = \tfrac{1}{2}(\chi_{\uparrow\uparrow} - \chi_{\downarrow\downarrow} - \chi_{\uparrow\downarrow} + \chi_{\downarrow\uparrow}). \tag{15}$$

For the corresponding bubble terms, we define

$$\chi_0 = \tfrac{1}{2}(\chi_{0\uparrow\uparrow} + \chi_{0\downarrow\downarrow}), \tag{16}$$

$$\overline{\chi}_0 = \tfrac{1}{2}(\chi_{0\uparrow\uparrow} - \chi_{0\downarrow\downarrow}). \tag{17}$$

Before we turn to illustrate the formalism of the Bethe-Salpeter equation, it is useful to shortly highlight some general properties of χ as a matrix in fermionic Matsubara frequency and charge-spin space. First of all, it is evident that in the SU(2)-symmetric PM phase, where $\chi_{\sigma\sigma'} = \chi_{-\sigma-\sigma'}$, the mixed charge and spin components vanish: $\chi_{sc} = \chi_{cs} = 0$. In general, at *ph* symmetry (half filling), χ_s, χ_c become real and bisymmetric matrices [17,19,51], while χ_{sc}, χ_{cs} become purely imaginary centro-Hermitian matrices [18,55] (cf. Fig. 2). Further, by exchanging $\nu \leftrightarrow \nu'$ (for $\omega = 0$), corresponding to a matrix transpose, we see that χ is a symmetric matrix $\chi^T = \chi$ (for details see Appendix A).

From these properties, it follows that while in the PM phase the eigenvalues λ_i of χ are purely real, in the AF phase they can either be real or appear in complex-conjugate pairs. Further, if χ is diagonalizable,[4] we find an orthonormal eigenbasis $\mathbf{v}_i$, where $\chi\mathbf{v}_i = \lambda_i\mathbf{v}_i$, with $\mathbf{v}_i^T\mathbf{v}_j = \delta_{ij}$. The corresponding eigenvectors $\mathbf{v}_i = (\boldsymbol{v}_i^s, \boldsymbol{v}_i^c)$ are either symmetric in Matsubara frequencies in the spin component $\boldsymbol{v}_i^s$ and antisymmetric in the charge component $\boldsymbol{v}_i^c$, or vice versa (this holds also in the AF phase; for a proof, refer to Appendix B). Since for the calculation of the physical response we sum over the Matsubara frequencies $(1/\beta)\sum_\nu \mathbf{v}_i$ (see Sec. II C), eigenvalues contribute solely to the physical charge or spin response, as the antisymmetric components vanish.

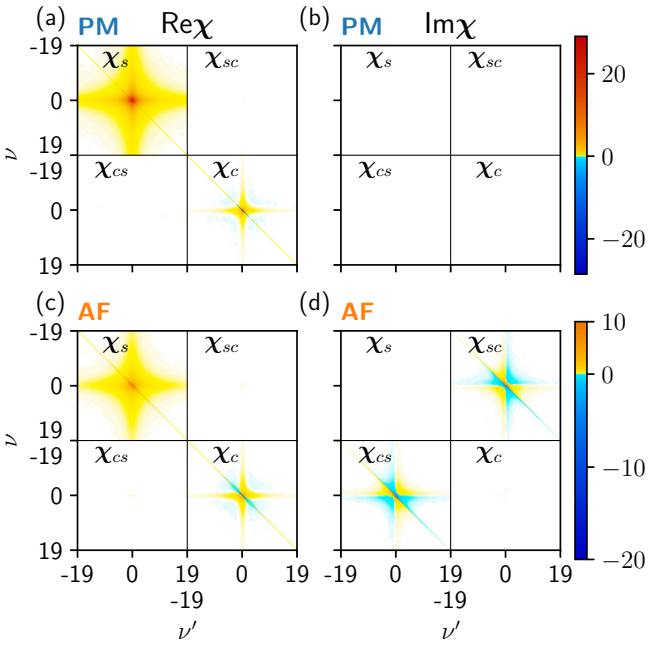


FIG. 2. Real (left column) and imaginary parts (right column) of the local generalized susceptibility χ calculated in DMFT for a Hubbard interaction value of $U = 3$ and temperature $T = 1/20$ at particle-hole symmetry ($\mu = U/2$). The top row shows the paramagnetic solution, and the bottom row the corresponding AF solution.

C. Static response and Bethe-Salpeter equation

When calculating the static physical responses of our system, we must recall that in a bipartite lattice, the $\mathbf{q}$-dependence of the density and magnetic operators,

$$\hat{n}_\alpha(\mathbf{q}) = \sum_\sigma \hat{n}_{\alpha\sigma}(\mathbf{q}) = \frac{1}{V}\sum_{\alpha\mathbf{k}\sigma} \hat{c}^\dagger_{\alpha\mathbf{k}\sigma}\hat{c}_{\alpha\mathbf{k}+\mathbf{q}\sigma}, \tag{18}$$

$$\hat{m}_\alpha(\mathbf{q}) = \hat{n}_{\alpha\uparrow}(\mathbf{q}) - \hat{n}_{\alpha\downarrow}(\mathbf{q}), \tag{19}$$

becomes periodic in the RBZ $[(-\pi/2, -\pi/2), (\pi/2, \pi/2))$. The full q-dependence in the BZ $[(-\pi, -\pi), (\pi, \pi))$ of the operators in the single atomic basis

$$\hat{n}(\mathfrak{q}) = \sum_\sigma \hat{n}_\sigma(\mathfrak{q}) = \frac{1}{\mathfrak{N}}\sum_{\mathbf{k}'\sigma} \hat{c}^\dagger_{\mathbf{k}'\sigma}\hat{c}_{\mathbf{k}'+\mathfrak{q}\sigma}, \tag{20}$$

$$\hat{m}(\mathfrak{q}) = \hat{n}_\uparrow(\mathfrak{q}) - \hat{n}_\downarrow(\mathfrak{q}), \tag{21}$$

[4]In principle, χ can become defective, and hence, not diagonalizable, at specific "exceptional points" in the phase diagram. For a detailed discussion, we refer the reader to Refs. [18,19].

where $\mathfrak{V} = 2V$ and $\mathbf{k}'$ runs here over the full BZ, can be restored by the two "band" expressions in the bipartite basis, corresponding to $\mathfrak{q} = \mathbf{q}$ and $\mathfrak{q} = \mathbf{q} + (\pi, \pi)$ of the single atomic basis [42]:

$$\hat{n}(\mathbf{q}) = \tfrac{1}{2}(\hat{n}_A(\mathbf{q}) + \hat{n}_B(\mathbf{q})), \tag{22}$$

$$\hat{n}(\mathbf{q} + (\pi, \pi)) = \tfrac{1}{2}(\hat{n}_A(\mathbf{q}) - \hat{n}_B(\mathbf{q})), \tag{23}$$

$$\hat{m}(\mathbf{q}) = \tfrac{1}{2}(\hat{m}_A(\mathbf{q}) + \hat{m}_B(\mathbf{q})), \tag{24}$$

$$\hat{m}(\mathbf{q} + (\pi, \pi)) = \tfrac{1}{2}(\hat{m}_A(\mathbf{q}) - \hat{m}_B(\mathbf{q})). \tag{25}$$

The static physical responses $\partial n(\mathfrak{q})/\partial\tilde{\mu}$, $\partial n(\mathfrak{q})/\partial h$, $\partial m(\mathfrak{q} + (\pi, \pi))/\partial\tilde{\mu}$, and $\partial m(\mathfrak{q} + (\pi, \pi))/\partial h$ to the external perturbations $\tilde{\mu}$ and h (at $\tilde{\mu} = 0$ and $h = 0$), which couple to $n(-\mathfrak{q})$ and $m(-\mathfrak{q} - (\pi, \pi))$, respectively, can then be calculated from the generalized susceptibilities [42]:[5,6]

$$\frac{1}{2}\left(\frac{\partial(n_A(\mathbf{q}) \pm n_B(\mathbf{q}))}{\partial\tilde{\mu}}\right) = \frac{1}{\beta^2}\sum_{\nu\nu'}\left(\chi^{AA}_{\mathbf{q}c} \pm \chi^{AB}_{\mathbf{q}c}\right), \tag{26}$$

$$\frac{1}{2}\left(\frac{\partial(n_A(\mathbf{q}) \pm n_B(\mathbf{q}))}{\partial h}\right) = \frac{1}{\beta^2}\sum_{\nu\nu'}\left(\chi^{AA}_{\mathbf{q}cs} \mp \chi^{AB}_{\mathbf{q}cs}\right), \tag{27}$$

$$\frac{1}{2}\left(\frac{\partial(m_A(\mathbf{q}) \mp m_B(\mathbf{q}))}{\partial\tilde{\mu}}\right) = \frac{1}{\beta^2}\sum_{\nu\nu'}\left(\chi^{AA}_{\mathbf{q}sc} \pm \chi^{AB}_{\mathbf{q}sc}\right), \tag{28}$$

$$\frac{1}{2}\left(\frac{\partial(m_A(\mathbf{q}) \mp m_B(\mathbf{q}))}{\partial h}\right) = \frac{1}{\beta^2}\sum_{\nu\nu'}\left(\chi^{AA}_{\mathbf{q}s} \mp \chi^{AB}_{\mathbf{q}s}\right). \tag{29}$$

These are obtained from the following Bethe-Salpeter equation [42] (see also Appendix C):

$$\boldsymbol{\chi}_{\mathbf{q}\pm} = \begin{pmatrix} \chi^{AA}_{\mathbf{q}s} \pm \chi^{AB}_{\mathbf{q}s} & \chi^{AA}_{\mathbf{q}sc} \mp \chi^{AB}_{\mathbf{q}sc} \\ \chi^{AA}_{\mathbf{q}cs} \pm \chi^{AB}_{\mathbf{q}cs} & \chi^{AA}_{\mathbf{q}c} \mp \chi^{AB}_{\mathbf{q}c} \end{pmatrix} = \left[\Gamma + \boldsymbol{\chi}^{-1}_{0\mathbf{q}\pm}\right]^{-1}, \tag{30}$$

where $\boldsymbol{\chi}^{-1}_{0\mathbf{q}\pm}$ is the corresponding "bubble" susceptibility and Γ is the irreducible vertex.

The former term is explicitly defined as

$$\boldsymbol{\chi}_{0\mathbf{q}\pm} = \begin{pmatrix} \chi^{AA}_{0\mathbf{q}} \pm \chi^{AB}_{0\mathbf{q}} & \overline{\chi}^{AA}_{0\mathbf{q}} \mp \overline{\chi}^{AB}_{0\mathbf{q}} \\ \overline{\chi}^{AA}_{0\mathbf{q}} \pm \overline{\chi}^{AB}_{0\mathbf{q}} & \chi^{AA}_{0\mathbf{q}} \mp \chi^{AB}_{0\mathbf{q}} \end{pmatrix}. \tag{31}$$

Further, we used the following notations:

$$\chi^{\alpha\alpha'}_{\mathbf{q}s} = \tfrac{1}{2}\left(\chi^{\alpha\alpha'}_{\mathbf{q}\uparrow\uparrow} + \chi^{\alpha\alpha'}_{\mathbf{q}\downarrow\downarrow} - \chi^{\alpha\alpha'}_{\mathbf{q}\uparrow\downarrow} - \chi^{\alpha\alpha'}_{\mathbf{q}\downarrow\uparrow}\right), \tag{32}$$

$$\chi^{\alpha\alpha'}_{\mathbf{q}sc} = \tfrac{1}{2}\left(\chi^{\alpha\alpha'}_{\mathbf{q}\uparrow\uparrow} - \chi^{\alpha\alpha'}_{\mathbf{q}\downarrow\downarrow} + \chi^{\alpha\alpha'}_{\mathbf{q}\uparrow\downarrow} - \chi^{\alpha\alpha'}_{\mathbf{q}\downarrow\uparrow}\right), \tag{33}$$

$$\chi^{\alpha\alpha'}_{\mathbf{q}c} = \tfrac{1}{2}\left(\chi^{\alpha\alpha'}_{\mathbf{q}\uparrow\uparrow} + \chi^{\alpha\alpha'}_{\mathbf{q}\downarrow\downarrow} + \chi^{\alpha\alpha'}_{\mathbf{q}\uparrow\downarrow} + \chi^{\alpha\alpha'}_{\mathbf{q}\downarrow\uparrow}\right), \tag{34}$$

$$\chi^{\alpha\alpha'}_{\mathbf{q}cs} = \tfrac{1}{2}\left(\chi^{\alpha\alpha'}_{\mathbf{q}\uparrow\uparrow} - \chi^{\alpha\alpha'}_{\mathbf{q}\downarrow\downarrow} - \chi^{\alpha\alpha'}_{\mathbf{q}\uparrow\downarrow} + \chi^{\alpha\alpha'}_{\mathbf{q}\downarrow\uparrow}\right), \tag{35}$$

$$\chi^{\alpha\alpha'}_{0\mathbf{q}} = \tfrac{1}{2}\left(\chi^{\alpha\alpha'}_{0\mathbf{q}\uparrow\uparrow} + \chi^{\alpha\alpha'}_{0\downarrow\downarrow}\right), \tag{36}$$

$$\overline{\chi}^{\alpha\alpha'}_{0\mathbf{q}} = \tfrac{1}{2}\left(\chi^{\alpha\alpha'}_{0\mathbf{q}\uparrow\uparrow} - \chi^{\alpha\alpha'}_{0\mathbf{q}\downarrow\downarrow}\right), \tag{37}$$

where the local generalized susceptibilities are denoted by omitting the $\mathbf{q}$ index. We note here that, due to the spontaneous breaking of the SU(2) symmetry associated with the AF ordering in the BSE of Eq. (30), the charge and the spin response of the two different "bands" (corresponding to $\mathbf{q}$ and $\mathbf{q} + (\pi, \pi)$) always couple to each other.

As for the irreducible vertex Γ, in the random phase approximation, it simply reads

$$\Gamma = \frac{1}{\beta^2}\begin{pmatrix} -U & 0 \\ 0 & U \end{pmatrix}, \tag{38}$$

while, in DMFT, it is formally defined as

$$\Gamma = \begin{pmatrix} \chi_s & \chi_{sc} \\ \chi_{cs} & \chi_c \end{pmatrix}^{-1} - \begin{pmatrix} \chi_0 & \overline{\chi}_0 \\ \overline{\chi}_0 & \chi_0 \end{pmatrix}^{-1}. \tag{39}$$

By taking a look at Eq. (39), we can readily note that the irreducible vertex Γ of DMFT may actually diverge, with the corresponding BSE becoming noninvertible if $\boldsymbol{\chi}$ has a zero eigenvalue $\lambda_i = 0$ [9,26]. In this case, as it is clearly discussed in the literature [10,13,16], techniques relying on the self-consistent resummation of a perturbative series of bold diagrams for $\Sigma[G]$ start to fail. In particular, the breakdown of self-consistent perturbation theory can be directly ascribed to the occurrence of the crossing between a physical and an unphysical solution [10,11,15,16,58] of the Luttinger Ward functional, $\Phi[G]$, which directly implies [13] the divergence of the irreducible vertex functions [9,17,26]. In fact, such a relation can also be understood, considering that the irreducible vertex is formally defined through the respective functional derivative of the self-energy functional $\Gamma = \beta\delta\Sigma[G]/\delta G$ [10,13], i.e., the second functional derivative of $\Phi[G]$. The corresponding definition of Γ in the bipartite basis explicitly reads

$$\Gamma = \frac{\beta}{2}\begin{pmatrix} \left(\frac{\delta\Sigma^{AA}_{\nu\uparrow}}{\delta G^{AA}_{\nu'\uparrow}} + \frac{\delta\Sigma^{AA}_{\nu\downarrow}}{\delta G^{AA}_{\nu'\downarrow}} - \frac{\delta\Sigma^{AA}_{\nu\uparrow}}{\delta G^{AA}_{\nu'\downarrow}} - \frac{\delta\Sigma^{AA}_{\nu\downarrow}}{\delta G^{AA}_{\nu'\uparrow}}\right) & \\ \left(\frac{\delta\Sigma^{AA}_{\nu\uparrow}}{\delta G^{AA}_{\nu'\uparrow}} - \frac{\delta\Sigma^{AA}_{\nu\downarrow}}{\delta G^{AA}_{\nu'\downarrow}} - \frac{\delta\Sigma^{AA}_{\nu\uparrow}}{\delta G^{AA}_{\nu'\downarrow}} + \frac{\delta\Sigma^{AA}_{\nu\downarrow}}{\delta G^{AA}_{\nu'\uparrow}}\right) & \\ \left(\frac{\delta\Sigma^{AA}_{\nu\uparrow}}{\delta G^{AA}_{\nu'\uparrow}} - \frac{\delta\Sigma^{AA}_{\nu\downarrow}}{\delta G^{AA}_{\nu'\downarrow}} + \frac{\delta\Sigma^{AA}_{\nu\uparrow}}{\delta G^{AA}_{\nu'\downarrow}} - \frac{\delta\Sigma^{AA}_{\nu\downarrow}}{\delta G^{AA}_{\nu'\uparrow}}\right) & \\ \left(\frac{\delta\Sigma^{AA}_{\nu\uparrow}}{\delta G^{AA}_{\nu'\uparrow}} + \frac{\delta\Sigma^{AA}_{\nu\downarrow}}{\delta G^{AA}_{\nu'\downarrow}} + \frac{\delta\Sigma^{AA}_{\nu\uparrow}}{\delta G^{AA}_{\nu'\downarrow}} + \frac{\delta\Sigma^{AA}_{\nu\downarrow}}{\delta G^{AA}_{\nu'\uparrow}}\right) & \end{pmatrix}. \tag{40}$$

Notably, a breakdown of the self-consistent perturbation theory has also been found in regimes where $\boldsymbol{\chi}$ shows only complex eigenvalues and Γ is formally not divergent [12,16,19,20]. More recently, in such cases one precise condition[7] limiting the applicability of self-consistent/iterative methods has been identified [59] as a corresponding sign

[5]Note that the responses $\partial n(\mathfrak{q} + (\pi, \pi))/\partial h = \partial[n_A(\mathbf{q}) \mp n_B(\mathbf{q})]/\partial h$ and $\partial m(\mathfrak{q})/\partial\tilde{\mu} = \partial[m_A(\mathbf{q}) \pm m_B(\mathbf{q})]/\partial\tilde{\mu}$ vanish due to the AF symmetry $(A, \sigma) \leftrightarrow (B, -\sigma)$.

[6]We note, in passing, that through the Ward identities [56,57] the eigenvectors of the generalized susceptibility $\boldsymbol{\chi}_{\mathbf{q}=0\pm}$ in Eq. (30) can also be regarded as spectral decomposition of the changes in the Green's function, e.g., $(1/2)\partial[\sum_\sigma(G^{AA}_{\nu\sigma} \pm G^{BB}_{\nu\sigma})]/\partial\tilde{\mu}$, $(1/2)\partial[\sum_\sigma(G^{AA}_{\nu\sigma} \pm G^{BB}_{\nu\sigma})]/\partial h$ [25].

[7]In particular, it has been demonstrated that this condition controls the stability of the physical fixed point of the iterative self-consistent perturbation theory, independently of the problem of the crossing of different branches of the Luttinger Ward functional.

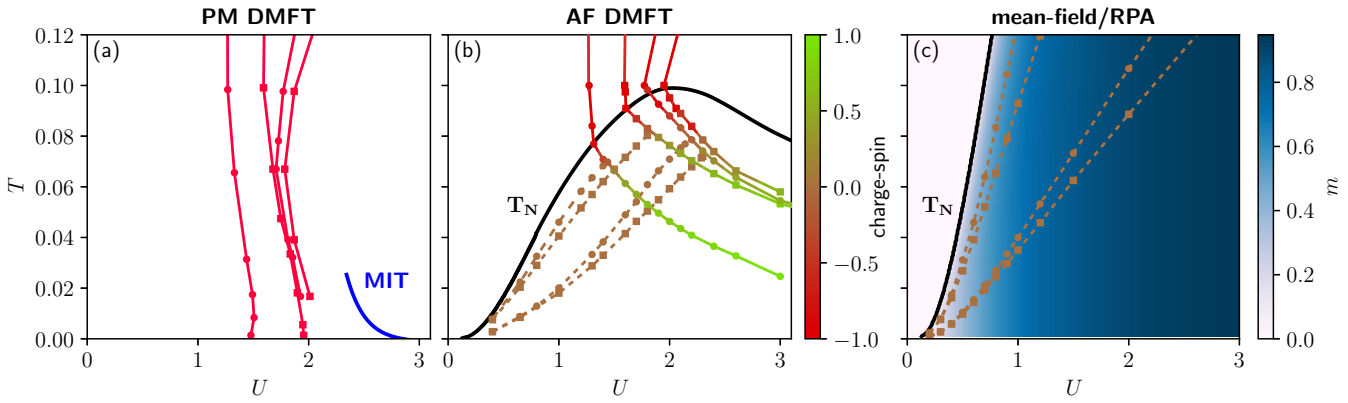


FIG. 3. Location of the first four divergences of the two-particle irreducible vertex Γ in the $T-U$ phase diagram for the PM DMFT solution in panel (a), the AF DMFT solution in panel (b), and the mean-field solution in panel (c) of the Hubbard model on a square lattice at half filling. The divergences correspond to a zero crossing of an eigenvalue $\lambda_i = 0$ of the local generalized susceptibility $\boldsymbol{\chi}$ denoted as lines in the $T-U$ phase diagram. The color of the lines in panels (a) and (b) indicates the dominant contribution of the eigenvector to the charge (red) or spin (green) component of $\boldsymbol{\chi}$, while parameter sets where only $\mathrm{Re}\,\lambda = 0$, but $\mathrm{Im}\,\lambda \neq 0$ (i.e., no divergence of the vertex), are displayed as brown dashed lines. (a) The divergence lines in the PM phase have been reproduced from Ref. [26]. The solid blue line marks U_{crit} of the paramagnetic Mott metal-to-insulator (MIT) transition, taken from Refs. [27,60]. (b) The black solid line indicates the Néel temperature T_N taken from Ref. [61], where the low U values have been estimated by the effective rescaled T_N of the mean-field solution based on Ref. [62], albeit with a slightly higher factor. (c) The background color scale shows the magnetization.

switch of the real part of an eigenvalue of

$$\mathfrak{X} = \begin{pmatrix} \boldsymbol{\chi}_0 & \overline{\boldsymbol{\chi}}_0 \\ \overline{\boldsymbol{\chi}}_0 & \boldsymbol{\chi}_0 \end{pmatrix}^{-1} \cdot \begin{pmatrix} \boldsymbol{\chi}_s & \boldsymbol{\chi}_{sc} \\ \boldsymbol{\chi}_{cs} & \boldsymbol{\chi}_c \end{pmatrix}. \tag{41}$$

At this point, it becomes convenient to also introduce the difference of the inverses of the two bubbles:

$$\begin{aligned} \Delta\boldsymbol{\chi}^{-1}_{0\mathbf{q}} &= \begin{pmatrix} \Delta\boldsymbol{\chi}^{-1}_{0\mathbf{q}+} & \Delta\overline{\boldsymbol{\chi}}^{-1}_{0\mathbf{q}-} \\ \Delta\overline{\boldsymbol{\chi}}^{-1}_{0\mathbf{q}+} & \Delta\boldsymbol{\chi}^{-1}_{0\mathbf{q}-} \end{pmatrix} \\ &= \begin{pmatrix} \boldsymbol{\chi}^{AA}_{0\mathbf{q}} + \boldsymbol{\chi}^{AB}_{0\mathbf{q}} & \overline{\boldsymbol{\chi}}^{AA}_{0\mathbf{q}} - \overline{\boldsymbol{\chi}}^{AB}_{0\mathbf{q}} \\ \overline{\boldsymbol{\chi}}^{AA}_{0\mathbf{q}} + \overline{\boldsymbol{\chi}}^{AB}_{0\mathbf{q}} & \boldsymbol{\chi}^{AA}_{0\mathbf{q}} - \boldsymbol{\chi}^{AB}_{0\mathbf{q}} \end{pmatrix}^{-1} - \begin{pmatrix} \boldsymbol{\chi}^{AA}_{0} & \overline{\boldsymbol{\chi}}^{AA}_{0} \\ \overline{\boldsymbol{\chi}}^{AA}_{0} & \boldsymbol{\chi}^{AA}_{0} \end{pmatrix}^{-1}. \end{aligned} \tag{42}$$

This allows to rewrite Eq. (30) with the help of Eq. (39) in a particularly insightful form for several DMFT applications:

$$\boldsymbol{\chi}_{\mathbf{q}\pm} = \left[\begin{pmatrix} \boldsymbol{\chi}_s & \boldsymbol{\chi}_{sc} \\ \boldsymbol{\chi}_{cs} & \boldsymbol{\chi}_c \end{pmatrix}^{-1} + \begin{pmatrix} \Delta\boldsymbol{\chi}^{-1}_{0\mathbf{q}\pm} & \Delta\overline{\boldsymbol{\chi}}^{-1}_{0\mathbf{q}\mp} \\ \Delta\overline{\boldsymbol{\chi}}^{-1}_{0\mathbf{q}\pm} & \Delta\boldsymbol{\chi}^{-1}_{0\mathbf{q}\mp} \end{pmatrix} \right]^{-1}. \tag{43}$$

In fact, within DMFT, $\Delta\boldsymbol{\chi}^{-1}_{0\mathbf{q}}$ can be regarded as the correction to the local generalized susceptibility $\boldsymbol{\chi}$ that is needed to obtain the lattice quantity $\boldsymbol{\chi}_{\mathbf{q}\pm}$. The convenience of such rewriting becomes clear if one observes that the $\mathbf{q}$-dependence enters here only in $\Delta\boldsymbol{\chi}^{-1}_{0\mathbf{q}}$.

III. DMFT RESULTS

A. Divergences of the irreducible vertex

Let us start by recalling the results of Refs. [9,26,27] that have investigated the divergences of the irreducible vertex Γ of the DMFT solution for the PM phase of the square lattice Hubbard model at *ph* symmetry. The location of the first four reported divergences is displayed by the red lines in the $T-U$ phase diagram in panel (a) of Fig. 3.

It should be underlined here that in the PM phase, as a result of the underlying SU(2) symmetry, $\boldsymbol{\chi}$ becomes block diagonal [44], resulting in fully separated charge and spin components $\boldsymbol{\chi}_s$ and $\boldsymbol{\chi}_c$. In this context [9,26,27], for positive U values (i.e., the case of a repulsive Hubbard model, considered here),[8] only $\boldsymbol{\chi}_c$[9] shows eigenvalues that cross zero ($\lambda_i = 0$) as a function of U; hence, only the charge component of Γ diverges. In particular, with increasing interaction values U, first an eigenvalue λ_i of $\boldsymbol{\chi}_c$ corresponding to an eigenvector $\mathbf{v}_i$ that is antisymmetric (in $\boldsymbol{v}^c_i$, with $\boldsymbol{v}^s_i = 0$) vanishes, while Γ diverges (illustrated by red solid line with circles), and becomes negative for any higher U value. By further increasing U, a second eigenvalue of $\boldsymbol{\chi}_c$, corresponding to a symmetric eigenvector, crosses zero (red solid line with squares). Eventually, for higher and higher values of U, more eigenvalues of $\boldsymbol{\chi}$ cross the zero line, with alternating symmetry of the eigenvector (red solid lines with circles for antisymmetric and squares for symmetric eigenvectors in $\boldsymbol{v}^c_i$). The resulting divergence lines in the $T-U$ phase diagram become denser with increasing U toward the Mott MIT transition (shown as blue line), which indeed represents an accumulation point of vertex divergences in the DMFT phase diagram [27].

Panel (b) of Fig. 3 illustrates, instead, how the situation changes when AF ordering is allowed in our DMFT calculations. In particular, below the Néel temperature T_N (black line), the SU(2) symmetry gets spontaneously broken. Hence, $\boldsymbol{\chi}$ must no longer be block diagonal and, indeed, it acquires nonzero imaginary components in its off-diagonal blocks $\boldsymbol{\chi}_{sc}$

[8]The situation for $U < 0$ at *ph* symmetry can be analytically mapped from $U > 0$ by a Shiba transformation. For details, we refer to Refs. [17,19].

[9]In fact, in the PM phase vertex divergences at *ph* symmetry and $U > 0$ appear in the charge and in the particle-particle channel, but *not* in the spin channel [9,12,26].

and $\boldsymbol{\chi}_{cs}$. In this situation, zero eigenvalues $\lambda_i = 0$ in $\boldsymbol{\chi}$ result in a divergence of Γ in the *overall* (coupled) spin-charge channel. Then, by following the first four divergence lines from the PM phase at higher temperatures into the AF phase below T_N, we observe a bending to higher values of U in the AF phase marked by an apparent "kink" at T_N, but without any discontinuity in accordance with the second-order nature of the phase transition. Differently, as in the PM phase, the eigenvectors associated with the zero eigenvalues thereby get a nonzero (imaginary) contribution in the spin component $\boldsymbol{v}_i^s$ (with opposite symmetry to $\boldsymbol{v}_i^c$). This mixing is illustrated by the color scale of the corresponding (solid) divergence line, which reflects the dominant contribution to the corresponding eigenvector $\mathbf{v}_i$, via the following expression of the respective spin-charge imbalance:

$$\mathcal{I}_{s-c} = \frac{\left|\boldsymbol{v}_i^{sT}\boldsymbol{v}_i^s\right| - \left|\boldsymbol{v}_i^{cT}\boldsymbol{v}_i^c\right|}{\left|\boldsymbol{v}_i^{sT}\boldsymbol{v}_i^s\right| + \left|\boldsymbol{v}_i^{cT}\boldsymbol{v}_i^c\right|}, \tag{44}$$

where -1 = red for charge, 1 = green for spin, and 0 = brown. In this way, it can be readily seen how for lower T and higher U values, $\boldsymbol{v}_i^s$ becomes more dominant (less red, more brown), until a second eigenvalue of $\boldsymbol{\chi}$, formally associated with a spin eigenvector in the PM phase ($\boldsymbol{v}_i^s \neq 0$, $\boldsymbol{v}_i^c = 0$) with the same eigenvector symmetry, becomes simultaneously zero, marking an "exceptional point" (EP), i.e., a degeneracy of the matrix. Precisely at that point, the eigenvector associated with the two zero eigenvalues shows no predominant contribution, with $\mathcal{I}_{s-c} = 0$ [19]. In passing the EP, one of the two eigenvalues remains zero, acquiring a dominant spin contribution in the eigenvector (solid green line), thus changing the nature of the formerly charge-dominated divergence line. This (now spin-dominated) vertex divergence line then continues toward higher U values approximately following the t^2/U behavior of T_N in the Heisenberg regime at strong coupling. In the same parameter regime, the second eigenvalue of the degenerate pairs at the EP, on the other hand, becomes negative, getting a charge-dominated $\mathbf{v}_i$.

At the same time, when moving from the EP toward $T = 0$ and $U = 0$ in the AF phase, the two eigenvalues become complex-conjugate pairs with $\mathrm{Re}\,\lambda_i = 0$ (and $\mathrm{Im}\,\lambda_i \neq 0$), shown as dashed brown lines. We will refer to the corresponding parameter sets as "real-part zero-crossing" (RZ) lines. Evidently, since their imaginary parts remain finite, they do not correspond to a divergence of Γ [16,19]. Furthermore, we note that this condition does not exactly coincide with one of the limiting criteria for the applicability of the self-consistent perturbation theory, which we reported in Eqs. (39) and (41). Hence, in general, it cannot be associated with its corresponding breakdown on a quantitative level. Nonetheless, their occurrence marks a sign change of the real part of the two conjugate eigenvalues from positive at higher T and lower U values to negative for lower T and higher U values, possibly relevant, as we will see, for the thermodynamic behavior of local charge (and spin) fluctuations. Moreover, as we will discuss later on, this analysis allows us to make plausible speculations on how the perturbative breakdown may occur in the actual two-dimensional case, when the SU(2) symmetry is restored.

In fact, as we will later investigate in Sec. III B, the parameter regions where the RZs take place qualitatively correspond to the small-U Slater region of the AF phase, while actual divergences occur in the large-U Heisenberg regime where magnetism arises from the ordering of local moments. Indeed, even before the more detailed investigation of Sec. III B, this interpretation is already supported by a quick comparison of RZs and vertex divergences in DMFT, with the corresponding ones in conventional MF/RPA theory [shown in panel (c) of Fig. 3], where only the Slater AF regime can be described. In the MF/RPA case, the local generalized susceptibility, to be compared with the DMFT one, is computed as [cf. Eq. (30)]

$$\boldsymbol{\chi} = \frac{1}{2V}\sum_{\mathbf{q}}(\boldsymbol{\chi}_{\mathbf{q}+} + \boldsymbol{\chi}_{\mathbf{q}-}). \tag{45}$$

As expected, since in MF/RPA the irreducible vertex Γ cannot diverge by construction [cf. Eq. (38)], no vertex divergence lines can be found. However, in the AF phase of the MF/RPA calculations, which has Slater nature, multiple RZ lines are found. These RZs, originating from the point with $T = 0$ and $U = 0$ and extending toward the region of $T \to \infty$ and $U \to \infty$, thus display an evident similarity with those found in the Slater regime of the DMFT AF phase.

Hence, from the overall analysis of Fig. 3, a rather definite picture emerges: Below T_N, one observes clear bending of the vertex divergence lines toward higher U values with respect to the corresponding PM phase, somewhat consistent with the expectation that the onset of a long-range order partly mitigates the correlation effects. At the same time, the appearance of similar RZ lines in the Slater regime of the DMFT AF as well as in MF/RPA indicates that, once the SU(2) symmetry is broken, the eigenvalues of $\boldsymbol{\chi}$ can acquire a negative real part (as they do in the strong-coupling PM regime) even in the parameter region accessible to perturbation theory, where no divergences of Γ occur.

B. Local charge response in Slater and Heisenberg regimes

To showcase the difference between the Slater and the Heisenberg AF, in Fig. 4 we compare the *local* static physical charge response $\chi_c = (1/\beta^2)\sum_{\nu\nu'}\boldsymbol{\chi}_c$ between the PM (blue circles) and AF phases (orange diamonds) as a function of temperature T for two different, representative interaction strengths. Specifically, to investigate the weak-coupling Slater regime, we take $U = 1$ in both MF/RPA (leftmost column) and DMFT (middle column), while for the strong-coupling Heisenberg regime, we fix $U = 3$ in our DMFT calculations (rightmost column).[10]

At $U = 1$, both MF/RPA and DMFT show a qualitative similar behavior of $\chi_c(T)$ [top row, panels (a) and (b), respectively]. In particular, when AF ordering is allowed, χ_c in the

[10]In DMFT, the local static physical charge response χ_c has been obtained from a direct measurement on the imaginary time axis, while in MF/RPA by analytical summation of the Matsubara frequencies. The respective contributions for χ_0 and $\sum_i \lambda_i^* w_i^{c*}$ (see the main text) were calculated through the summation of a finite Matsubara frequency box—accounting for the high-frequency asymptotics in χ_0.

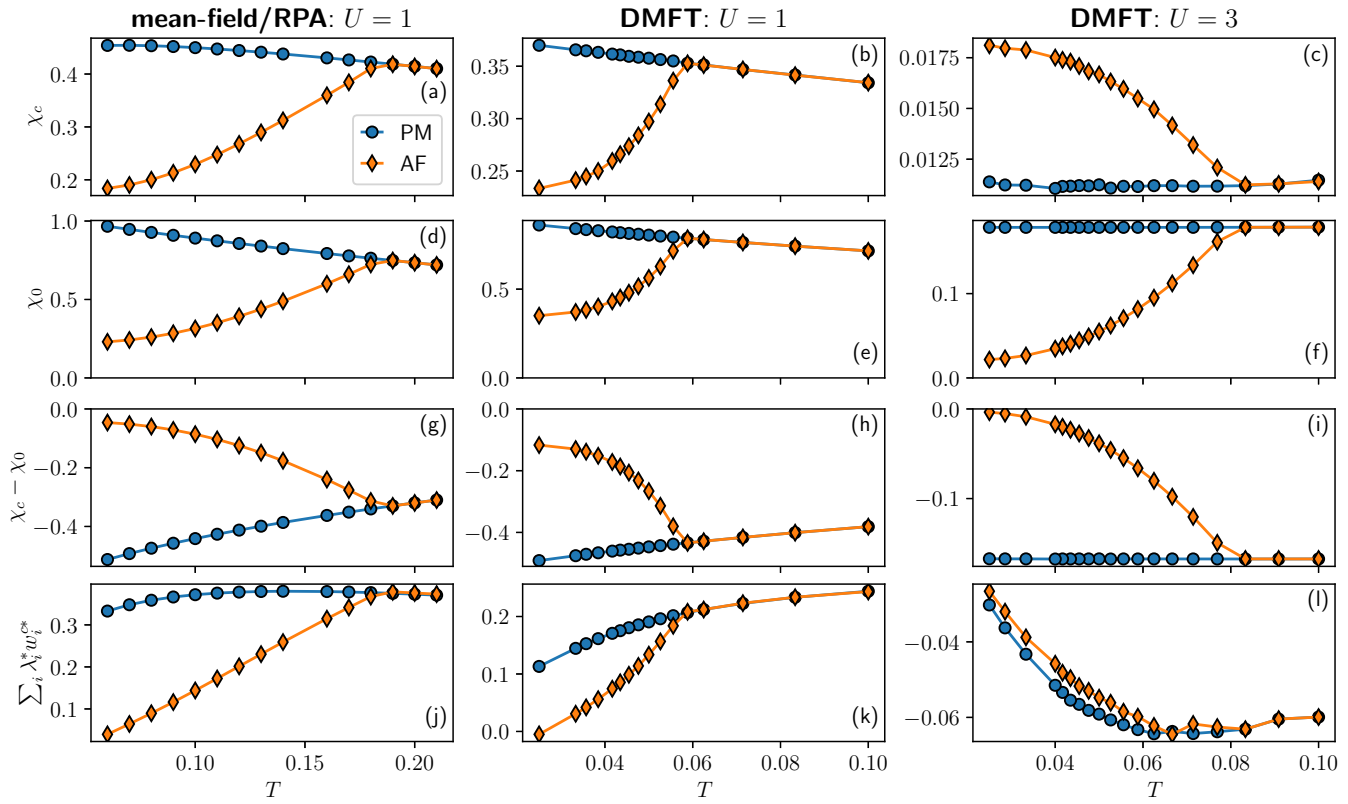


FIG. 4. Comparison of the local charge response χ_c and of its different diagrammatic contributions as a function of temperature T in our AF (orange diamonds) and PM (blue circles) calculations for weak coupling $U = 1$ in mean field/RPA (left column) and DMFT (middle column), as well as for strong coupling $U = 3$ in DMFT (right column). Top row: Local charge response χ_c. Second-top row: Bubble contribution χ_0 to χ_c. Second-bottom row: The difference between the bubble contributions χ_0 and χ_c, corresponding to the vertex corrections. Bottom row: Contributions of the eigenvalues λ_i^* times corresponding weights w_i^{c*}—associated with the lowest Matsubara frequencies—to χ_c.

AF phase appears to always decrease in comparison to the corresponding PM solutions.[11]

However, while in MF/RPA the qualitative behavior observed at $U = 1$ persists for all interaction values of U (not shown), the situation gets reversed in DMFT. Specifically, at strong coupling [$U = 3$, top row, panel (c)], we observe that, although χ_c is significantly lower than that for weak coupling, the AF ordering visibly enhances the *local* charge response with respect to the PM solution. Such an enhancement can be indeed regarded as a characteristic hallmark of the Heisenberg AF physics, being associated with the kinetic energy gain in the AF state [38,63] that arises from the onset of the AF coherence between preformed local magnetic moments.

In order to trace the origin of the different behavior of $\chi_c(T)$ between the weak-coupling Slater and strong-coupling Heisenberg AF phase at the two-particle level, we start by separating the contributions to $\chi_c(T)$ into the local "bubble" term $\chi_0 = (1/\beta^2)\sum_{\nu\nu'} \boldsymbol{\chi}_0$, which excludes any contribution from the two-particle scattering vertex, and the "rest" $\chi_c - \chi_0 = \chi_{\text{vert}}$, which entails all vertex corrections. We see that in *both* Slater ($U = 1$) and Heisenberg regimes ($U = 3$), the bubble contribution χ_0 is positive and becomes suppressed in the AF solution compared to the PM solution (second row in Fig. 4). The vertex corrections χ_{vert}, instead, are negative in both regimes (also in MF/RPA) and become *less negative* in the AF phase (third row in Fig. 4). Since bubble and vertex contributions share a similar behavior at weak and strong coupling, what actually controls the qualitative behavior of the physical response χ_c is the delicate balance between the two contributions χ_0 and χ_{vert} and, in particular, whether the bubble χ_0 or the vertex χ_{vert} plays the dominant role.

More insight can be gained by looking at the different eigenvalue contributions of $\boldsymbol{\chi}$ to χ_c:

$$\chi_c = \sum_i \lambda_i w_i^c, \tag{46}$$

where we introduced the weights of the eigenvalues to the charge sector:

$$w_i^c = \left(\frac{1}{\beta}\sum_\nu \boldsymbol{v}_i^c\right)^2. \tag{47}$$

Before proceeding, an important observation should be made: For large values of the Matsubara frequencies $\nu, \nu' \to \infty$, the vertex corrections to the generalized susceptibility decay faster than the corresponding bubble term. Hence, $\boldsymbol{\chi}_c$

[11] A similar behavior (see Appendix G) can be observed in the local spin response $\chi_s(T)$. In contrast to the charge response, as we will subsequently discuss, the local spin response $\chi_s(T)$ also decreases at strong coupling $U = 3$ with respect to the PM solution.

becomes asymptotically $\boldsymbol{\chi}_0$ [51], i.e., a diagonal matrix $\propto \delta_{\nu\nu'}$. Thus, for these frequency values, we find corresponding $\boldsymbol{\chi}$ eigenvalues with eigenvectors localized at high frequencies and essentially indistinguishable from those of $\boldsymbol{\chi}_0$. Conversely, the contribution of the vertex corrections enters the eigenvalues, whose eigenvectors have a domain concentrated at low frequencies. Evidently, for those, both the vertex and $\boldsymbol{\chi}_0$ will contribute. Hence, they are the ones responsible for differentiating the Slater and Heisenberg physics. In the bottom row of Fig. 4, we compare, between the PM and AF phases, the χ_c contributions of the eigenvalues λ_i^* of $\boldsymbol{\chi}$ associated with eigenvectors with the lowest Matsubara frequency domains. In particular, the eigenvalues λ_i^* of the eigenvectors $\boldsymbol{v}_i^{c*}$ that have a maximum absolute value at the lowest five Matsubara frequencies

$$-5 \leqslant \arg\max_{n(\nu)} \left|\boldsymbol{v}_i^{c*}\right| < 5 \tag{48}$$

have been considered. At weak coupling $U = 1$ (in MF/RPA and DMFT), the respective contributions $\sum_i \lambda_i^* w_i^{c*}$ show a qualitative similarity to the behavior of χ_0: They are positive in the PM phase and are getting suppressed in the AF phase. At the same time, in DMFT at strong coupling, $\sum_i \lambda_i^* w_i^{c*}$ resembles *qualitatively* the vertex χ_{vert}: It is *negative* in the PM phase, but becomes *less* negative in the AF phase, contributing to the observed (relative) enhancement of $\chi_c(T)$ below T_N. While the quantitative behavior of $\chi_c(T)$ cannot be rigorously reproduced without including a higher number of eigenvectors in Eq. (48), our result demonstrates how this (low-frequency) quantity already well captures the physical change occurring between the Slater and the Heisenberg AF, on a qualitative level. This observation paves the way for a thorough analysis of the eigenvalue spectrum of $\boldsymbol{\chi}$ in the different physical regimes.

C. Eigenvalues of the local generalized susceptibility matrix

In order to trace the hallmarks of the Slater and Heisenberg physics in the eigenspectrum of $\boldsymbol{\chi}$, in Fig. 5 we compare the eigenvalues of the PM (top row) and AF (bottom row) solutions between weak ($U = 1$, left column) and strong coupling ($U = 3$, right column) for a representative temperature ($T = 1/30$). The color of the eigenvalues indicates the individual contributions (multiplied by their respective weights w_i^c) to the local charge response, while the specific eigenvalues λ_i^*—used for the analysis in the bottom row of Fig. 4—have been marked by black circles. Here, we see that the qualitatively different behavior of the contributions of λ_i^* between weak and strong coupling is already present at the level of the individual eigenvalues.

At weak coupling, $\boldsymbol{\chi}$ (or $\boldsymbol{\chi}_c$) has only positive eigenvalues in the PM phase [panel (a), the vertex divergence lines have not been crossed], and the contributions of λ_i^* are positive. In the AF phase [panel (c)], we see complex-conjugate pairs, with a negative real part (stemming from the crossing of the RZ lines), which suppress the local charge response.

Conversely, at strong coupling for $U = 3$, in the PM [panel (b)] many vertex divergence lines have already been crossed, and hence, many negative eigenvalues are present. These lead to negative λ_i^* contributions, which suppress χ_c. In the AF

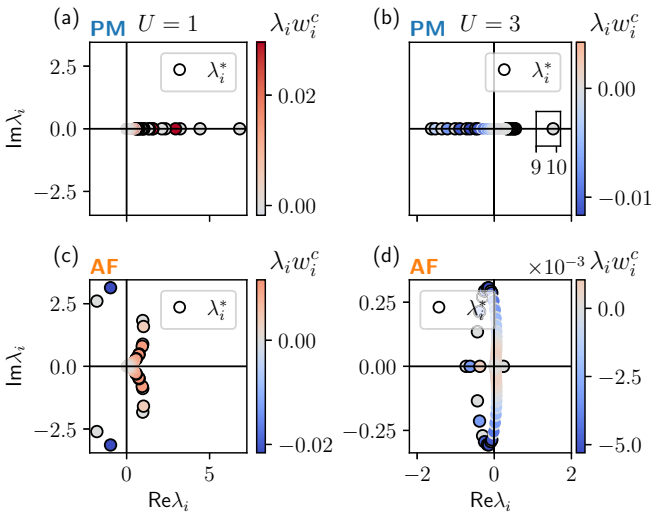


FIG. 5. Eigenvalues of the local generalized susceptibility matrix $\boldsymbol{\chi}$ computed by means of DMFT, in the PM (top row) and AF (bottom row) phases for weak $U = 1$ (left column) and strong $U = 3$ (right column) coupling at $T = 1/30$. The eigenvalues λ_i^*, whose eigenvectors are associated with the lowest Matsubara frequencies, have been marked by black circles. The coloring shows the respective contribution to the local charge response χ_c.

phase [panel (d)], as a result of the spontaneous breaking of the SU(2) symmetry, some of the negative real eigenvalues become complex-conjugate pairs. However, all of them get a *significantly less negative* real part with respect to their PM counterpart, leading to the observed enhancement of the λ_i^* contributions below T_N.

These considerations about the results shown in Fig. 5 clarify the role played by the negative eigenvalues of $\boldsymbol{\chi}$ in driving the physical behavior from the Slater to the Heisenberg regime. In particular, the appearance of negative eigenvalues of $\boldsymbol{\chi}$ (or, more precisely, of $\boldsymbol{\chi}_c$) in the PM phase appears to be the key ingredient for triggering an emerging AF order with Heisenberg nature: The negative real eigenvalues of the PM phase induce [12,13,21,24] the strong suppression of on-site charge fluctuations typical of a bad-metal/Mott insulating regime, while the breaking of the SU(2) symmetry below T_N progressively reduces their negative components, featuring the slight rebound of $\chi_c(T)$ characteristic of the Heisenberg-AF regime.[12] This conclusion can be further supported by analytical considerations in the context of the Bethe lattice; see Appendix E for details.

We complete our analysis of the local generalized charge susceptibility $\boldsymbol{\chi}_c$, by taking a look at the different eigenvalue λ_i evolutions in temperature T between weak ($U = 1$, left column) and strong coupling ($U = 3$, right column) when entering the AF phase in Fig. 6. At weak coupling, lowering T (left column, from top to bottom) and entering

[12]The contrary conclusion cannot be made. The atomic limit of the Hubbard model has negative eigenvalues in $\boldsymbol{\chi}_c$, but shows no enhancement of the local charge response χ_c, when explicitly breaking the SU(2) symmetry by turning on an external magnetic field (see Appendix F).

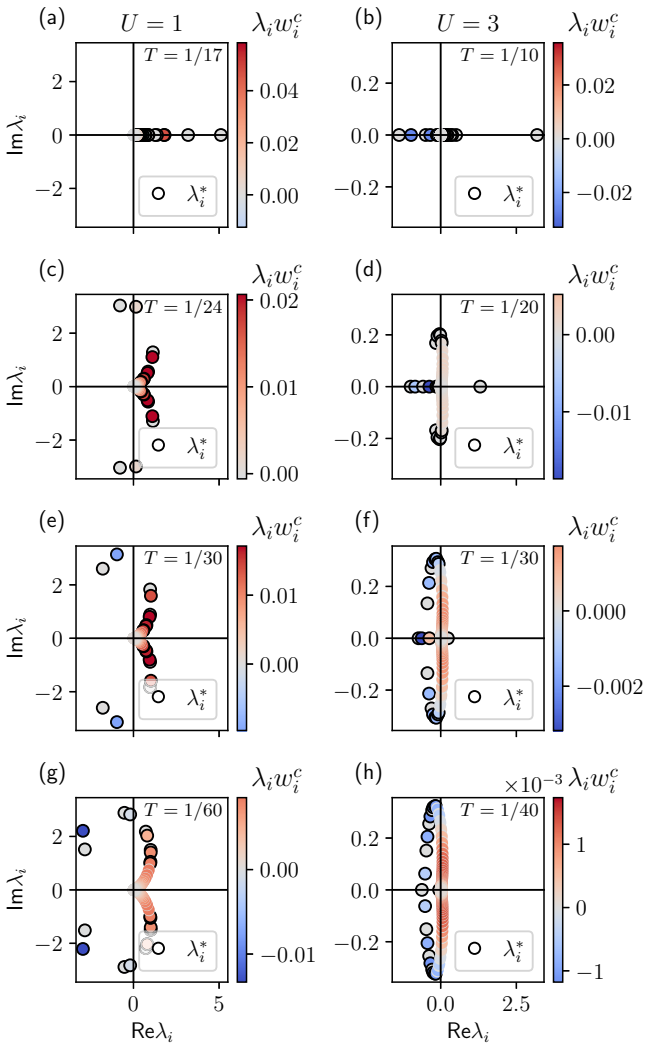


FIG. 6. Similar to Fig. 5: Calculated DMFT eigenvalues of the local generalized susceptibility matrix $\boldsymbol{\chi}$ for weak $U = 1$ (left column) and strong $U = 3$ coupling (right column) for various temperatures above (first row) and below (second-to-fourth row) the corresponding T_N.

the AF phase [panels (c)–(g)] leads to the development of complex-conjugate pairs of eigenvalues, which then appear to be disposed in a sort of "fountain"-like structure in the representation of Fig. 6. By crossing several RZ lines, more and more of them start to develop a negative real part.

At strong coupling, the behavior is more complex: Starting from negative values in the PM phase at high temperature [$T = 1/10$, panel (b)] and reducing the temperature (right column, top to bottom) leads, below T_N [panels (d)–(h)], to the emergence of similar "fountain"-like structure as at weak coupling, albeit with a relevant difference: Not all eigenvalues of $\boldsymbol{\chi}$ become immediately complex-conjugate pairs at the breaking of the SU(2) symmetry. In particular, the most negative eigenvalues of the PM phase stay, at first, real also below T_N, but become progressively less negative. At the same time, also the most positive real eigenvalues of $\boldsymbol{\chi}$ with a predominant spin contribution of their associated eigenvectors remain real below T_N. Their value, however, gets gradually suppressed, until they cross zero at spin-dominated vertex divergence lines [greenish lines in panel (b) of Fig. 3]. By further reducing the temperature, these eigenvalues become negative[13] until they eventually meet the previously discussed negative real eigenvalues. Their merging gives rise to the formation of complex-conjugate pairs. The largest real eigenvalue colored in gray provides, indeed, a good example of this general behavior in the right column of Fig. 6. It is also interesting to emphasize that this specific eigenvalue mostly contributes to the enhanced Curie-like static magnetic response of the PM bad-metallic/Mott phase [17]. Hence, it encodes, within the spin scattering channel, a significant aspect of the local moment physics, which underlies the onset of a Heisenberg AF instability. Quite remarkably, it is precisely the vanishing of this eigenvalue in the strong-coupling AF phase that determines the appearance of the first vertex divergence line with a predominant spin nature in the Heisenberg regime of the AF phase.

IV. BSE IN THE AF PHASE: AN EIGENVALUE PERSPECTIVE

In Refs. [18,20,25,64,65], in the context of DMFT, the eigenvalues of the static local generalized susceptibility $\boldsymbol{\chi}$ have been successfully linked to the values of the uniform ($\mathrm{q} = 0$) and/or staggered [$\mathrm{q} = (\pi, \pi, \ldots)$] linear response of the lattice system considered. In particular, it was demonstrated that the largest positive and lowest negative eigenvalues of the local $\boldsymbol{\chi}$ could directly trigger actual thermodynamic instabilities. It is thus natural to ask, to what extent these findings generalize to the AF phase of the bipartite lattice. To this aim, we start by recalling that, within DMFT, the BSE in the PM phase—for both spin and charge susceptibilities—takes the following form [20,35,64] [cf. Eq. (43)]:

$$\boldsymbol{\chi}_{\mathrm{q}c/s} = \left[\boldsymbol{\chi}_{c/s}^{-1} + \Delta\boldsymbol{\chi}_{0\mathrm{q}}^{-1}\right]^{-1}. \tag{49}$$

Here, all quantities are defined on the single atomic basis; hence, q runs over the full BZ, and we defined $\Delta\boldsymbol{\chi}_{0\mathrm{q}}^{-1} = \boldsymbol{\chi}_{0\mathrm{q}}^{-1} - \boldsymbol{\chi}_{0}^{-1}$—analog to the bipartite lattice. For the Bethe lattice case (in the infinite coordination limit, with rescaled nearest-neighboring hopping t), Eq. (49) becomes particularly intriguing, as its explicit expression connects [20,35] directly the eigenvalues $\lambda_i^{c/s}$ of the local quantity $\boldsymbol{\chi}_{c/s}$ with the eigenvalues $\lambda_i^{\mathrm{q}c/s}$ of $\boldsymbol{\chi}_{\mathrm{q}}$ [20,25,35,64,66]:

$$\boldsymbol{\chi}_{\mathrm{q}=(0,0,\ldots)c/s} = \left[\boldsymbol{\chi}_{c/s}^{-1} + \frac{t^2}{\beta}\mathbb{1}\right]^{-1}, \tag{50}$$

$$\boldsymbol{\chi}_{\mathrm{q}=(\pi,\pi,\ldots)c/s} = \left[\boldsymbol{\chi}_{c/s}^{-1} - \frac{t^2}{\beta}\mathbb{1}\right]^{-1}, \tag{51}$$

[13] We note that these negative real eigenvalues with a predominant spin contribution, when real and antisymmetric in v_i^s, and imaginary and symmetric in v_i^c, actually also do contribute enhancing to the charge response $\lambda_i w_i^c$.

$$\lambda_i^{\mathbf{q}=(0,0,\dots)c/s} = \left(\frac{1}{\lambda_i^{c/s}} + \frac{t^2}{\beta}\right)^{-1}, \tag{52}$$

$$\lambda_i^{\mathbf{q}=(\pi,\pi,\dots)c/s} = \left(\frac{1}{\lambda_i^{c/s}} - \frac{t^2}{\beta}\right)^{-1}. \tag{53}$$

An eigenvalue $1/\lambda_i^{c/s}$ reaching $\pm t^2/\beta$ thus triggers a divergence of $\lambda_i^{\mathbf{q},c/s}$ and, if the corresponding weight $w_i^{c/s}$ is finite, also a divergence of the corresponding physical response:

$$\chi_{\mathbf{q}c/s} = \frac{1}{\beta^2}\sum_{\nu\nu'} \boldsymbol{\chi}_{\mathbf{q}c/s} = \sum_i \lambda_i^{\mathbf{q}c/s} w_i^{c/s}. \tag{54}$$

Therefore, in the PM phase, $1/\lambda_i^s \to t^2/\beta$ is responsible for the divergence of the AF spin response at the AF phase transition [64] and $1/\lambda_i^c \to -t^2/\beta$ for the divergence of the derivative of the double occupancy $\partial D/\partial U$ [25], as well as for the divergence of the uniform charge response at the critical point of the MIT away from *ph* symmetry [18,20,66]. For the case of the square lattice of interest in this study, Eqs. (50)–(53) have been numerically found to hold approximately [20,67] by replacing $t \to t_{\text{eff}}(\mu, \beta, U)$ with an effective constant that depends on the system parameters, with a good agreement to the Bethe lattice expression in the intermediate-to-strong coupling regime.

We now generalize these relations to the DMFT solution for the AF phase in a bipartite lattice. As we show in Appendix E, in the Bethe lattice, Eq. (43) explicitly reads

$$\boldsymbol{\chi}_{\mathbf{q}=0\pm} = \left[\begin{pmatrix} \boldsymbol{\chi}_s & \boldsymbol{\chi}_{sc} \\ \boldsymbol{\chi}_{cs} & \boldsymbol{\chi}_c \end{pmatrix}^{-1} \pm \frac{t^2}{\beta}\begin{pmatrix} \mathbb{1} & 0 \\ 0 & -\mathbb{1} \end{pmatrix}\right]^{-1}, \tag{55}$$

featuring the direct generalization of the PM expressions of Eqs. (50) and (51).

As a next step, the evaluation of $\Delta\boldsymbol{\chi}^{-1}_{0\mathbf{q}=0}$ for the bipartite square lattice in Fig. 7 at different values of U shows that similarly as in the PM phase, also in the AF phase, the Bethe lattice expression in Eq. (55) (with the rescaled hopping $4t^2/\beta$ in two dimensions [67]) becomes a good approximation at intermediate-to-strong coupling.

Given this result, it would then be tempting to search for an analogous direct connection between the eigenvalues of the local $\boldsymbol{\chi}$ and the lattice response $\boldsymbol{\chi}_{\mathbf{q}=0\pm}$ such as the one valid in the PM phase. However, due to the σ_z-like structure of $\Delta\boldsymbol{\chi}^{-1}_{0\mathbf{q}=0}$, which ultimately originates from the checkerboard pattern of the AF order on the bipartite lattice, the identification of a so direct link is no longer possible. In fact, in contrast to the case of a true multiorbital system and/or of a ferromagnetic order [25] (where instead of a Pauli matrix σ_z structure, one simply has the identity $\mathbb{1}$), in the AF-DMFT case, it is not possible to diagonalize simultaneously the two terms on the right-hand side of Eq. (55).

Nonetheless, at small values of the magnetization m, when $\boldsymbol{\chi}_{sc}$ and $\boldsymbol{\chi}_{cs}$ are small compared to $\boldsymbol{\chi}_s$ and $\boldsymbol{\chi}_c$, we can employ a different strategy: We transform Eq. (55) into the eigenbasis of the respective subspaces of the local spin $\boldsymbol{\chi}_s\tilde{\boldsymbol{v}}_i^s = \lambda_i^s\tilde{\boldsymbol{v}}_i^s$ and

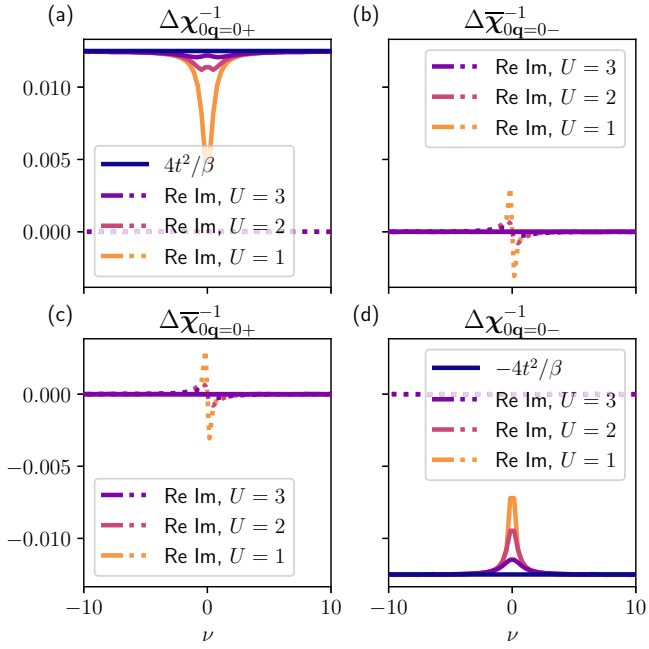


FIG. 7. Difference of the inverse uniform and local bubble $\Delta\boldsymbol{\chi}^{-1}_{0\mathbf{q}=0}$ as a function of $\nu = \nu'$ in the AF phase of the square lattice Hubbard model solved in DMFT for different values of the Hubbard interaction from weak $U = 1$ to strong $U = 3$ coupling at temperature $T = 1/20$.

charge $\boldsymbol{\chi}_c\tilde{\boldsymbol{v}}_i^c = \lambda_i^c\tilde{\boldsymbol{v}}_i^c$ susceptibilities:

$$\begin{pmatrix} \tilde{\boldsymbol{v}}_i^s & 0 \\ 0 & \tilde{\boldsymbol{v}}_i^c \end{pmatrix}^T \boldsymbol{\chi}_{\mathbf{q}=0\pm}\begin{pmatrix} \tilde{\boldsymbol{v}}_j^s & 0 \\ 0 & \tilde{\boldsymbol{v}}_j^c \end{pmatrix}$$
$$= \left[\begin{pmatrix} \lambda_i^s\delta_{ij} & \lambda_{ij}^{sc} \\ \lambda_{ji}^{sc} & \lambda_i^c\delta_{ij} \end{pmatrix}^{-1} \pm \frac{1}{\beta}\begin{pmatrix} t^2 & 0 \\ 0 & -t^2 \end{pmatrix}\delta_{ij}\right]^{-1}, \tag{56}$$

where it should be noted that, while $(\tilde{\boldsymbol{v}}_i^s, 0)$ and $(0, \tilde{\boldsymbol{v}}_i^c)$ are not eigenvectors of the general $\boldsymbol{\chi}$ matrix, they do form an orthonormal basis set. Then, if two subspace eigenvectors $(\tilde{\boldsymbol{v}}_i^s, 0)$, $(0, \tilde{\boldsymbol{v}}_i^c)$ span the same eigenvector space as two eigenvectors $\mathbf{v}_i$ of the total $\boldsymbol{\chi}\mathbf{v}_i = \lambda_i\mathbf{v}_i$, we have

$$\tilde{\boldsymbol{v}}_i^{sT}\boldsymbol{\chi}_{sc}\tilde{\boldsymbol{v}}_j^c = \lambda_{ij}^{sc} \approx \lambda_i^{sc}\delta_{ij}, \tag{57}$$

$$\tilde{\boldsymbol{v}}_i^{cT}\boldsymbol{\chi}_{cs}\tilde{\boldsymbol{v}}_j^s = \left(\tilde{\boldsymbol{v}}_j^{sT}\boldsymbol{\chi}_{sc}\tilde{\boldsymbol{v}}_i^c\right)^T = \lambda_{ji}^{sc} \approx \lambda_i^{sc}\delta_{ji}, \tag{58}$$

where λ_{ij}^{sc} becomes purely imaginary at *ph* symmetry.

In Fig. 8, we can verify, via our DMFT calculations, that this approximation actually holds for small values of the magnetization m [panel (a)] and that, hence, the BSE equation can be separated into distinct 2×2 matrix equations. As expected, the approximation breaks down with increasing m, because, then, larger clusters of subspace eigenvectors couple to each other.

After having verified the condition under which the approximation in Eqs. (57) and (58) holds, let us shortly discuss their consequences in the regime of its applicability. The

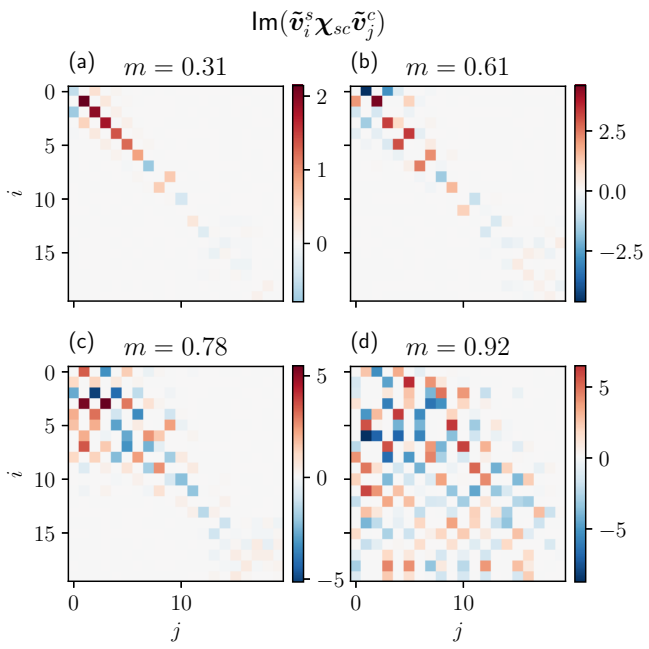


FIG. 8. $\mathrm{Im}(\tilde{\boldsymbol{v}}_i^s \boldsymbol{\chi}_{sc} \tilde{\boldsymbol{v}}_j^c)$: Imaginary part of the projection of the symmetry breaking local generalized $\boldsymbol{\chi}_{sc}$ susceptibility onto the eigenvectors $\tilde{\boldsymbol{v}}_i^s, \tilde{\boldsymbol{v}}_i^c$ of $\boldsymbol{\chi}_s$ and $\boldsymbol{\chi}_c$ for interaction value $U = 3$ and with increasing magnetization m at temperatures $T = (1/13, 1/15, 1/18, 1/30)$. One can easily notice how the approximated relation of Eqs. (57) and (58) holds reasonably well for small m, while it deteriorates for large magnetization values.

right-hand side of Eq. (56) would yield

$$\frac{D_i \delta_{ij}}{\left(\frac{1}{\lambda_i^s} \pm \frac{t^2}{\beta} D_i\right)\left(\frac{1}{\lambda_i^c} \mp \frac{t^2}{\beta} D_i\right) - \left(\frac{\lambda_i^{sc}}{\lambda_i^s \lambda_i^c}\right)^2} \times \begin{pmatrix} \frac{1}{\lambda_i^c} \mp \frac{t^2}{\beta} D_i & \frac{\lambda_i^{sc}}{\lambda_i^s \lambda_i^c} \\ \frac{\lambda_i^{sc}}{\lambda_i^s \lambda_i^c} & \frac{1}{\lambda_i^s} \pm \frac{t^2}{\beta} D_i \end{pmatrix}, \tag{59}$$

where

$$D_i = 1 - \frac{\left(\lambda_i^{sc}\right)^2}{\lambda_i^s \lambda_i^c}. \tag{60}$$

Here, we can immediately notice that in the AF phase, the hopping constant $t^2 \to t^2 D_i$ appears as if it were effectively renormalized in the BSE. At the same time, even taking into account such renormalization, one could no longer directly apply analogous instability conditions as in the PM phase, such as

$$\frac{1}{\lambda_i^s} \pm \frac{t^2}{\beta} D_i = 0, \tag{61}$$

$$\frac{1}{\lambda_i^c} \mp \frac{t^2}{\beta} D_i = 0, \tag{62}$$

due to the finite offset $-(\lambda_i^{sc}/\lambda_i^s \lambda_i^c)^2$. On the contrary, quite interestingly, an instability for $\lambda_i^{sc} \neq 0$ can now only appear simultaneously both in the spin and in the charge component of the BSE, when the following relation holds:

$$\left(\frac{1}{\lambda_i^s} \pm \frac{t^2}{\beta} D_i\right)\left(\frac{1}{\lambda_i^c} \mp \frac{t^2}{\beta} D_i\right) - \left(\frac{\lambda_i^{sc}}{\lambda_i^s \lambda_i^c}\right)^2 = 0. \tag{63}$$

We note here that when approaching the phase transition, the magnetic order reduces sufficiently fast to yield $\lambda_i^{sc} \to 0$ and $D_i \sim \mathcal{O}[(\lambda_i^{sc})^2] \to 1$, so that the AF instability condition

$$\frac{1}{\lambda_i^s} - \frac{t^2}{\beta} = 0 \tag{64}$$

coincides in the AF and PM phases. This implies that, when approaching the magnetic transition in the AF phase for $\lambda_i^{sc} \to 0$, where the AF condition in Eq. (64) is fulfilled, also the off-diagonal components in Eq. (59) can be expected to diverge. In contrast, the charge component, for $\lambda_i^c \neq -\beta/t^2$, remains finite. We want to emphasize here that while these considerations rigorously hold only in the limit of small m, the main effects of the SU(2)-symmetry breaking in the BSE for the AF phase [i.e., (1) a sizable renormalization of t^2 term and (2) a global instability condition that differs from the PM ones] can be expected to have a general validity.

At particle-hole symmetry, however, due to the coupled symmetry of the eigenvectors for $\boldsymbol{\chi}_{\mathbf{q}=0\pm}$ (either symmetric in spin $\boldsymbol{v}_i^s$ and antisymmetric in charge $\boldsymbol{v}_i^c$, or vice versa), the instability of one eigenvalue of $\boldsymbol{\chi}_{\mathbf{q}=0\pm}$ can occur only for the charge or spin sector: its effects will be, thus, *not* transmitted to the other physical response functions in Eqs. (26)–(29), since the antisymmetric components vanish in the Matsubara sum. For finite doping instead, where particle-hole symmetry is violated, formerly antisymmetric eigenvectors acquire a symmetric part [18] and do contribute to the physical response functions [20,25]. There, a simultaneous instability in both the spin and charge responses can be expected. Possibly, this occurs due to a similar mechanism as in Ref. [20].

V. CONCLUSIONS

In this work, we have presented a thorough investigation of the divergences of the irreducible vertex functions in the presence of a spontaneously broken SU(2) symmetry. This way, we lifted one of the limitations of literature studies [9–12,14–18,20–27,68–70] on the breakdown of the many-electron self-consistent perturbation theory, which were hitherto restricted to paramagnetic phases.

In particular, we performed DMFT calculations on the two-particle level in the AF phase of the half filled (particle-hole symmetric) Hubbard model, from weak to intermediate-to-strong coupling, determining the location and the nature of the divergences of the irreducible vertex functions in the $T-U$ phase diagram of the problem.

The main findings of our analysis can be summarized as follows:

(1) The onset of the AF long-range order tends to mitigate the occurrence of divergences in the irreducible vertex functions: For decreasing temperatures and for increasing values of the staggered magnetization, their location gets progressively shifted toward larger values of U with respect to the underlying paramagnetic phase.

(2) In the AF phase, due to the spontaneous breaking of the SU(2) symmetry, the charge and the longitudinal sectors of

the Bethe Salpeter equation for the generalized susceptibility χ become coupled [19,42,44]. Hence, below T_N, the nature of the corresponding vertex divergencies acquires a mixed character. In particular, our analysis of the eigenvectors associated with vanishing eigenvalues of χ (and hence with the vertex divergencies) indicates that right below T_N, the vertex divergencies display a predominating charge character (prevalently red colored lines in Fig. 3), similar to the one they had in the PM phase. However, when reducing the temperature further, this character abruptly changes into a dominating longitudinal spin one (prevalently green colored lines in Fig. 3) after the occurrence of an exceptional point.

Quite significantly, the above-mentioned exceptional point is found when the largest eigenvalue of χ in the spin sector of the PM solution, responsible [17] for the characteristic Curie behavior of the physical magnetic response in the Mott phase, is damped down to zero for increasing value of the magnetization. This provides a direct link between observed vertex divergencies in the AF phase and the physics of the local moment formation.

(3) From any exceptional point, an RZ line (where the real part of a pair of complex-conjugate eigenvalues of χ is zero, albeit with a finite imaginary part) departs toward the origin of the $T-U$ phase diagram.

As a consequence of (1)–(3), the AF phase diagram of the Hubbard model in DMFT gets roughly split into two parts with respect to the irreducible vertex properties: At weak coupling, below T_N, only RZ lines are present, qualitatively similar to those we found in the (static) RPA calculations. Actual vertex divergences, systematically shifted to larger U values with respect to the PM phase, are found, instead, in the intermediate-to-strong coupling regime.

The qualitative difference in the two-particle properties gets directly reflected in the different nature of the AF phases in the two regimes (Slater at weak coupling versus Heisenberg at strong coupling), as demonstrated by our comparative analysis of the contributions of the eigenvalues/eigenvectors of χ to the behavior of the respective local static charge response.

While the DMFT expressions relating the eigenspectrum properties of the local χ to the physical response of the lattice system become more complicated than in the SU(2)-symmetric case [18,20,25,35,71], at temperatures slightly below T_N (i.e., for small values of the staggered magnetization m) physically transparent approximations could be derived and successfully tested. These might be useful, e.g., to investigate the occurrence of phase-separation instabilities in the AF-phase out-of-half filling [72–74]. This latter topic has indeed a long history related to the proposal that phase separation can be a crucial driving force of the cuprate phase diagram as a function of doping, leading to both charge-density-wave ordering and superconductivity itself [75]. In this regard, an analysis based on two-particle properties can shed light on the role of magnetism and of the reduced dimensionality [76] in driving the phase-separation instability and in its relation with superconductivity.

VI. OUTLOOK

The results obtained in our study have several implications, both for future algorithmic developments and for a more fundamental understanding of the many-electron theory and the effect of symmetry breaking on its properties.

From an algorithmic perspective, the distinct properties of two-particle DMFT vertex functions in the weak- and strong-coupling regimes—encoding the differences between Slater and Heisenberg antiferromagnets—offer valuable insights for generalizing diagrammatic extensions of DMFT [40], such as DΓA [77] and DMF^{2}RG [78,79], to study AF-ordered phases [42,80].

In particular, our findings indicate the necessity to choose, as local input for diagrammatic resummations beyond DMFT, local two-particle vertex functions *directly* calculated in the corresponding AF-ordered phase. In fact, if one stabilized the AF instabilities only through diagrammatic resummations built on a PM DMFT input, essential aspects of the nonperturbative AF physics (such as the crossover from Slater to Heisenberg [37,38]) would be completely absent in the theoretical description.

From a more physical viewpoint, RZ lines are present in both the AF solution of RPA and the weak-coupling/Slater regime of DMFT, displaying an exponential behavior down to $T = U = 0$. This provides—as we will detail in the following—intriguing hints on possible nonperturbative features of the putative exact solution of two-dimensional systems [81]. There, due to the Mermin-Wagner theorem [82], the onset of an AF order will be confined to the ground state, while, at finite T, the ordered phase will be replaced by a regime of quasi-long-range [83,84] (i.e., with an exponentially growing magnetic correlation length [85–88]) AF fluctuations. In this situation, the "formally" preserved SU(2) symmetry of our (particle-hole symmetric) problem will render χ a real symmetric matrix, block diagonal in the charge and in the spin sector, with a purely real eigenvalue spectrum. As a consequence, the expected suppression of the charge response by strong (long-range) AF fluctuations [89] can no longer be realized through the same mechanism as in the Slater regime described by the "perturbative" RPA. There, the SU(2)-symmetry breaking, allowing for eigenvalues with nonzero imaginary part, leads to the "fountain structure" visible in Figs. 5 and 6, which suppresses the charge fluctuations. In the exact 2D solution, which fulfills the Mermin-Wagner theorem, the lack of long-range order will suppress the imaginary parts of the eigenvalues. In that case, the progressive reduction of on-site charge fluctuations will plausibly occur through the true vanishing of purely real eigenvalues.

Hence, the RZ lines found in the Slater regime would transform into actual divergence lines. In this respect, it would then be plausible to expect, in the exact solution of the two-dimensional Hubbard model, an accumulation of vertex divergence lines toward $T = U = 0$, with a qualitatively similar (exponential) shape as the RZ lines in our AF phase diagram of the DMFT solution. In fact, such expectation would also be consistent with the trend of the very few existing cluster-DMFT [36] studies [12,16] of vertex divergencies in the PM phase of the two-dimensional Hubbard model, which showed an evident shift of the divergence lines toward lower U values with respect to the corresponding DMFT calculations.

Evidently, such speculations call for future, systematic cluster-DMFT investigations of the 2D Hubbard model on

the two-particle level and the application of the more recently introduced methods [46,47] that restore the Mermin-Wagner theorem, starting from a symmetry-broken (dynamical) mean-field solution. In particular, the verification of such a scenario would provide a clear indication, in a rigorous theoretical framework, for a complete vanishing of the convergence radius of the self-consistent perturbation theory for the (particle-hole symmetric) two-dimensional Hubbard model in the zero-temperature limit.

ACKNOWLEDGMENTS

We thank P. Chalupa-Gantner, H. Eßl, E. Moghadas, P. Oberleitner, S. Rohshap, G. Sangiovanni, and D. Springer for helpful comments and discussion. M.C. acknowledges financial support from the National Recovery and Resilience Plan (NRRP) MUR Projects No. CN00000013-ICSC and No. PE0000023-NQSTI and by MUR via PRIN 2020 (Prot. 2020JLZ52N 002) and PRIN 2022 (Prot. 20228YCYY7) programs. M.R. acknowledges support as a recipient of a DOC Fellowship of the Austrian Academy of Sciences. This research was also funded by the Austrian Science Fund (FWF) via 10.55776/I5487 (M.R.) and 10.55776/I5868, Project No. P1 of the research unit FOR 5249 of the German research foundation (DFG) (A.T.). Calculations have been performed on the Vienna Scientific Cluster (VSC).

DATA AVAILABILITY

A dataset containing all numerical data and plot scripts used to generate the figures of this publication is publicly available [90].

APPENDIX A: SYMMETRY OF THE STATIC GENERALIZED SUSCEPTIBILITY

At *ph* symmetry (half filling), the generalized susceptibility in Eq. (6) is invariant under exchanging creation and annihilation operators with opposite spin $\hat{c}^{\dagger}_{\alpha\sigma} \leftrightarrow \hat{c}_{\alpha-\sigma}$ also in the AF phase [19]. Hence, any summation of opposite spin components $\chi_{\sigma\sigma'} + \chi_{-\sigma-\sigma'}$ becomes a real and bisymmetric matrix in Matsubara frequencies [17,19,51]. Therefore, χ_s, χ_c become real and bisymmetric matrices, while χ_{sc}, χ_{cs}, composed of the opposite spin component differences, become purely imaginary centro-Hermitian matrices [18,55] at *ph* symmetry (nonzero in the AF phase). Away from *ph* symmetry, all, χ_s, χ_c, χ_{sc}, and χ_{cs}, become complex centro-Hermitian matrices.

Further, by exchanging $\nu \leftrightarrow \nu'$ (for $\omega = 0$), corresponding to a matrix transpose, the spin components in Eq. (6) are exchanged, leading to $\chi^T_{\sigma\sigma'} = \chi_{\sigma'\sigma}$. From this and the considerations above, we conclude that χ is (1) a symmetric $\chi^T = \chi$ and (2) a κ-real matrix [18,19,91]:

$$\Pi\chi\Pi = \begin{pmatrix} J\chi_s J & J\chi_{sc}J \\ J\chi_{cs}J & J\chi_c J \end{pmatrix} = \begin{pmatrix} \chi_s^* & \chi_{sc}^* \\ \chi_{cs}^* & \chi_c^* \end{pmatrix} = \chi^*, \quad \text{(A1)}$$

at *ph* symmetry

$$\Pi\chi\Pi = \begin{pmatrix} \chi_s & -\chi_{sc} \\ -\chi_{cs} & \chi_c \end{pmatrix} = \chi^*, \quad \text{(A2)}$$

with

$$\Pi = \begin{pmatrix} J & 0 \\ 0 & J \end{pmatrix} \quad \text{(A3)}$$

being a permutation matrix and $J := \delta_{\nu(-\nu')}$.

APPENDIX B: SYMMETRY OF THE EIGENVECTORS AT *ph* SYMMETRY

At *ph* symmetry, the generalized susceptibility in the longitudinal channel

$$\chi = \begin{pmatrix} \chi_s & \chi_{sc} \\ \chi_{cs} & \chi_c \end{pmatrix} \quad \text{(B1)}$$

consists of two bisymmetric real submatrices $\chi_s = J\chi_s J$, $\chi_c = J\chi_c J$ and of two pure imaginary centro-Hermitian submatrices $\chi_{sc} = -J\chi_{sc}J$, $\chi_{cs} = -J\chi_{cs}J$, with $\chi_{sc} = \chi_{cs}^T$, where $J := \delta_{\nu(-\nu')}$. Hence, we can further split the submatrices into the following 2×2 blocks [19]:

$$\chi = \begin{pmatrix} A & JBJ & E & -JFJ \\ B & JAJ & F & -JEJ \\ E & F & C & JDJ \\ -JFJ & -JEJ & D & JCJ \end{pmatrix}. \quad \text{(B2)}$$

Let us formally split the eigenvectors $\mathbf{v}_i$ of χ, $\chi\mathbf{v}_i = \lambda_i\mathbf{v}_i$, into symmetric and antisymmetric parts:

$$\mathbf{v}_i = \begin{pmatrix} s_i^s \\ Js_i^s \\ s_i^c \\ Js_i^c \end{pmatrix} + \begin{pmatrix} a_i^s \\ -Ja_i^s \\ a_i^c \\ -Ja_i^c \end{pmatrix}, \quad \text{(B3)}$$

leading to

$$\begin{aligned} \chi\mathbf{v}_i &= \begin{pmatrix} (A+JB)s_i^s + (E+JF)a_i^c \\ J\big[(A+JB)s_i^s + (E+JF)a_i^c\big] \\ (C-JD)a_i^c + (E+JF)s_i^s \\ -J\big[(C-JD)a_i^c + (E+JF)s_i^s\big] \end{pmatrix} \\ &\quad + \begin{pmatrix} (A-JB)a_i^s + (E-JF)s_i^c \\ -J\big[(A-JB)a_i^s + (E-JF)s_i^c\big] \\ (C+JD)s_i^c + (E-JF)a_i^s \\ J\big[(C+JD)s_i^c + (E-JF)a_i^s\big] \end{pmatrix} \\ &= \lambda_i \left[\begin{pmatrix} s_i^s \\ Js_i^s \\ a_i^c \\ -Ja_i^c \end{pmatrix} + \begin{pmatrix} a_i^s \\ -Ja_i^s \\ s_i^c \\ Js_i^c \end{pmatrix} \right]. \end{aligned} \quad \text{(B4)}$$

Here, we see that the combination of symmetric in spin and antisymmetric in charge, or vice versa, keeps the symmetry when multiplied with χ. Since those two realizations are intrinsically orthogonal to each other, both vectors (if nonzero) must be separate eigenvectors of χ. Hence, every eigenvector

of an orthogonal basis is either

$$\mathbf{v}_i = \begin{pmatrix} \boldsymbol{s}_i^s \\ \boldsymbol{J}\boldsymbol{s}_i^s \\ \boldsymbol{a}_i^c \\ -\boldsymbol{J}\boldsymbol{a}_i^c \end{pmatrix} \quad \text{or} \quad \mathbf{v}_i = \begin{pmatrix} \boldsymbol{a}_i^s \\ -\boldsymbol{J}\boldsymbol{a}_i^s \\ \boldsymbol{s}_i^c \\ \boldsymbol{J}\boldsymbol{s}_i^c \end{pmatrix}. \tag{B5}$$

APPENDIX C: PHYSICAL BASIS OF THE BSE IN THE LONGITUDINAL CHANNEL

Here, we briefly review the necessary transformations to obtain the BSE in Eq. (30) from the BSE in the microscopical basis of the atomic and spin indices [42]. In the longitudinal channel, the BSE reads

$$\boldsymbol{\chi}^{\alpha\alpha'}_{\mathbf{q}\sigma\sigma'} = \left[\begin{pmatrix} \Gamma^{AA}_{\uparrow\uparrow} & \Gamma^{AA}_{\uparrow\downarrow} & \Gamma^{AB}_{\uparrow\uparrow} & \Gamma^{AB}_{\uparrow\downarrow} \\ \Gamma^{AA}_{\downarrow\uparrow} & \Gamma^{AA}_{\downarrow\downarrow} & \Gamma^{AB}_{\downarrow\uparrow} & \Gamma^{AB}_{\downarrow\downarrow} \\ \Gamma^{BA}_{\uparrow\uparrow} & \Gamma^{BA}_{\uparrow\downarrow} & \Gamma^{BB}_{\uparrow\uparrow} & \Gamma^{BB}_{\uparrow\downarrow} \\ \Gamma^{BA}_{\downarrow\uparrow} & \Gamma^{BA}_{\downarrow\downarrow} & \Gamma^{BB}_{\downarrow\uparrow} & \Gamma^{BB}_{\downarrow\downarrow} \end{pmatrix} - \begin{pmatrix} \boldsymbol{\chi}^{AA}_{0\mathbf{q}\uparrow\uparrow} & \mathbf{0} & \boldsymbol{\chi}^{AB}_{0\mathbf{q}\uparrow\uparrow} & \mathbf{0} \\ \mathbf{0} & \boldsymbol{\chi}^{AA}_{0\mathbf{q}\downarrow\downarrow} & \mathbf{0} & \boldsymbol{\chi}^{AB}_{0\mathbf{q}\downarrow\downarrow} \\ \boldsymbol{\chi}^{BA}_{0\mathbf{q}\uparrow\uparrow} & \mathbf{0} & \boldsymbol{\chi}^{BB}_{0\mathbf{q}\uparrow\uparrow} & \mathbf{0} \\ \mathbf{0} & \boldsymbol{\chi}^{BA}_{0\mathbf{q}\downarrow\downarrow} & \mathbf{0} & \boldsymbol{\chi}^{BB}_{0\mathbf{q}\downarrow\downarrow} \end{pmatrix}^{-1} \right]^{-1}. \tag{C1}$$

By using the symmetry $(A,\sigma) \leftrightarrow (B,-\sigma)$, the matrices in the BSE show a centrosymmetric property in atomic and spin indices of the following form:

$$\mathcal{C} = \begin{pmatrix} \boldsymbol{A} & \boldsymbol{B} \\ \boldsymbol{J}\boldsymbol{B}\boldsymbol{J} & \boldsymbol{J}\boldsymbol{A}\boldsymbol{J} \end{pmatrix}, \tag{C2}$$

where $\boldsymbol{A}$ and $\boldsymbol{B}$ are submatrices and

$$\boldsymbol{J} = \begin{pmatrix} \mathbf{0} & \mathbb{1} \\ \mathbb{1} & \mathbf{0} \end{pmatrix}. \tag{C3}$$

$\mathcal{C}$ can be block diagonalized via

$$\mathcal{Q}\mathcal{C}\mathcal{Q}^T = \begin{pmatrix} \boldsymbol{A}-\boldsymbol{B}\boldsymbol{J} & \mathbf{0} \\ \mathbf{0} & \boldsymbol{A}+\boldsymbol{B}\boldsymbol{J} \end{pmatrix}, \tag{C4}$$

with

$$\mathcal{Q} = \frac{1}{\sqrt{2}} \begin{pmatrix} \mathbb{1} & -\boldsymbol{J} \\ \mathbb{1} & \boldsymbol{J} \end{pmatrix}. \tag{C5}$$

This gives us two independent BSE equations:

$$\begin{aligned} \left(\mathcal{Q}\boldsymbol{\chi}^{\alpha\alpha'}_{\mathbf{q}\sigma\sigma'}\mathcal{Q}^T\right)_\pm &:= \boldsymbol{A} \pm \boldsymbol{B}\boldsymbol{J} \\ &= \left[\begin{pmatrix} \Gamma^{AA}_{\uparrow\uparrow} \pm \Gamma^{AB}_{\uparrow\downarrow} & \Gamma^{AA}_{\uparrow\downarrow} \pm \Gamma^{AB}_{\uparrow\uparrow} \\ \Gamma^{AA}_{\downarrow\uparrow} \pm \Gamma^{AB}_{\downarrow\downarrow} & \Gamma^{AA}_{\downarrow\downarrow} \pm \Gamma^{AB}_{\downarrow\uparrow} \end{pmatrix} - \begin{pmatrix} \boldsymbol{\chi}^{AA}_{0\mathbf{q}\uparrow\uparrow} & \pm\boldsymbol{\chi}^{AB}_{0\mathbf{q}\uparrow\uparrow} \\ \pm\boldsymbol{\chi}^{AB}_{0\mathbf{q}\downarrow\downarrow} & \boldsymbol{\chi}^{AA}_{0\mathbf{q}\downarrow\downarrow} \end{pmatrix}^{-1} \right]^{-1}. \end{aligned} \tag{C6}$$

Applying the similarity transformation $\boldsymbol{U}(\mathcal{Q}\boldsymbol{\chi}^{\alpha\alpha'}_{\mathbf{q}\sigma\sigma'}\mathcal{Q}^T)_\pm\boldsymbol{U}^T$ with

$$\boldsymbol{U} = \frac{1}{\sqrt{2}} \begin{pmatrix} \mathbb{1} & -\mathbb{1} \\ \mathbb{1} & \mathbb{1} \end{pmatrix} \tag{C7}$$

then leads to the physical basis of Eq. (30).

APPENDIX D: BSE IN THE BETHE LATTICE

In the Bethe lattice with infinite lattice connectivity (where DMFT is exact), the BSE equation develops a simple and intuitive form due to the semicircular density of states $\rho(\epsilon) = (1/2\pi t^2)\sqrt{4t^2-\epsilon^2}$. In the following, we will first rederive the corresponding expression for the PM ($\zeta_{\nu\uparrow} = \zeta_{\nu\downarrow}$) phase (see also Refs. [20,25,35,64,92]) and extend them to the AF phase later on.

1. PM phase

For the subsequent derivation, it is convenient to express the local Green's function G_ν of the Bethe lattice as Hilbert transform:

$$G_{\nu\sigma} = \int_{-\infty}^{\infty} d\epsilon\, \rho(\epsilon) \frac{1}{\zeta_{\nu\sigma}-\epsilon} = \frac{1}{\zeta_{\nu\sigma} - t^2 G_{\nu\sigma}}, \tag{D1}$$

with the hybridization function $\Delta_{\nu\sigma} = t^2 G_{\nu\sigma}$ and $\zeta_{\nu\sigma} = \mathrm{i}\nu + \mu - \Sigma_{\nu\sigma}$. The local "bubble" susceptibility χ_0 reads

$$\boldsymbol{\chi}_0 = -\beta G^2_{\nu\sigma}\delta_{\nu\nu'} \tag{D2}$$

and the uniform ($\mathbf{q}=0$) "bubble" susceptibility $\boldsymbol{\chi}_{0\mathbf{q}=0}$ of the lattice is

$$\boldsymbol{\chi}_{0\mathbf{q}=0} = -\beta \int_{-\infty}^{\infty} d\epsilon\, \rho(\epsilon) \frac{\delta_{\nu\nu'}}{(\zeta_{\nu\sigma}-\epsilon)^2} = \beta \frac{dG_{\nu\sigma}}{d\zeta_{\nu\sigma}}\delta_{\nu\nu'}. \tag{D3}$$

With the help of Eq. (D1), we get

$$\frac{dG_{\nu\sigma}}{d\zeta_{\nu\sigma}} = -\frac{G^2_{\nu\sigma}}{1-t^2G^2_{\nu\sigma}} \tag{D4}$$

and, hence, obtain for the BSE of the uniform generalized lattice susceptibility $\boldsymbol{\chi}_{\mathbf{q}=0c/s}$ the following form:

$$\begin{aligned} \boldsymbol{\chi}_{\mathbf{q}=0c/s} &= \left[\Gamma_{c/s} + \boldsymbol{\chi}^{-1}_{0\mathbf{q}=0}\right]^{-1} \\ &= \left[\boldsymbol{\chi}^{-1}_{c/s} - \boldsymbol{\chi}^{-1}_0 + \boldsymbol{\chi}^{-1}_{0\mathbf{q}=0}\right]^{-1} = \left[\boldsymbol{\chi}^{-1}_{c/s} + \frac{t^2}{\beta}\mathbb{1}\right]^{-1}, \end{aligned} \tag{D5}$$

where $\Gamma_{c/s} = \boldsymbol{\chi}^{-1}_{c/s} - \boldsymbol{\chi}^{-1}_0$ is the local two-particle irreducible vertex and $\boldsymbol{\chi}_{c/s}$ the local generalized susceptibility in charge or spin.

2. AF phase

In the AF phase, the Green's function becomes a matrix of the two sublattice sites $\alpha = (A,B)$:

$$\begin{aligned} G_{\nu\sigma} &= \int_{-\infty}^{\infty} d\epsilon\, \rho(\epsilon) \frac{1}{\zeta_{A\nu\sigma}\zeta_{B\nu\sigma} - \epsilon^2} \begin{pmatrix} \zeta_{B\nu\sigma} & \epsilon \\ \epsilon & \zeta_{A\nu\sigma} \end{pmatrix} \\ &= \begin{pmatrix} G_{A\nu\sigma} & 0 \\ 0 & G_{B\nu\sigma} \end{pmatrix} = \begin{pmatrix} \frac{1}{\zeta_{A\nu\sigma} - t^2 G_{B\nu\sigma}} & 0 \\ 0 & \frac{1}{\zeta_{B\nu\sigma} - t^2 G_{A\nu\sigma}} \end{pmatrix} \end{aligned} \tag{D6}$$

and the local "bubble" susceptibility $\boldsymbol{\chi}_0$ reads

$$\boldsymbol{\chi}^{\alpha\alpha}_{0\sigma\sigma} = -\beta G^2_{\alpha\nu\sigma}\delta_{\nu\nu'}. \tag{D7}$$

The respective $\boldsymbol{\chi}_{0\mathbf{q}=0}$ susceptibilities become

$$\boldsymbol{\chi}^{\alpha\alpha}_{0\mathbf{q}=0\sigma\sigma} = -\beta\int_{-\infty}^{\infty} d\epsilon\,\rho(\epsilon)\frac{\zeta^2_{\bar{\alpha}\nu\sigma}\delta_{\nu\nu'}}{(\zeta_{\alpha\nu\sigma}\zeta_{\bar{\alpha}\nu\sigma}-\epsilon^2)^2}, \tag{D8}$$

$$\boldsymbol{\chi}^{AB}_{0\mathbf{q}=0\sigma\sigma} = -\beta\int_{-\infty}^{\infty} d\epsilon\,\rho(\epsilon)\frac{\epsilon^2\delta_{\nu\nu'}}{(\zeta_{A\nu\sigma}\zeta_{B\nu\sigma}-\epsilon^2)^2}, \tag{D9}$$

where for $\alpha = A$, $\bar{\alpha} = B$, or vice versa. With the definition of

$$g_\nu(\lambda) = \int_{-\infty}^{\infty} d\epsilon\,\rho(\epsilon)\frac{1}{\zeta_{A\nu\sigma}\zeta_{B\nu\sigma}-(\lambda\epsilon)^2} \tag{D10}$$

$$= \frac{1}{\zeta_{A\nu\sigma}\zeta_{B\nu\sigma}(1-(\lambda t)^2 g_\nu(\lambda))} = \frac{G_{\alpha\nu\sigma}}{\zeta_{\bar{\alpha}\nu\sigma}},$$

$$g_\nu := g_\nu(\lambda = 1), \tag{D11}$$

we can reexpress the susceptibilities with

$$\boldsymbol{\chi}^{\alpha\alpha}_{0\mathbf{q}=0\sigma\sigma} = \beta\zeta_{\bar{\alpha}\nu\sigma}\frac{dg_\nu}{d\zeta_{\alpha\nu\sigma}}\delta_{\nu\nu'} = -\beta\frac{G^2_{\alpha\nu\sigma}}{1-\varrho^2_\nu}\delta_{\nu\nu'}, \tag{D12}$$

$$\boldsymbol{\chi}^{AB}_{0\mathbf{q}=0\sigma\sigma} = -\frac{\beta}{2}\frac{dg_\nu(\lambda)}{d\lambda}\bigg|_{\lambda=1}\delta_{\nu\nu'} = -\beta\frac{\varrho_\nu g_\nu}{1-\varrho_\nu}\delta_{\nu\nu'}$$

$$= -\beta\frac{\varrho^2_\nu}{t^2(1-\varrho^2_\nu)}\delta_{\nu\nu'}, \tag{D13}$$

where $\varrho_\nu = t^2 G_{A\nu\sigma}G_{B\nu\sigma}$ and we used $1+\varrho_\nu = g_\nu\zeta_{A\nu\sigma}\zeta_{B\nu\sigma}$. By considering the AF symmetry $(A,\sigma)\leftrightarrow(B,-\sigma)$, we can greatly simplify the $\boldsymbol{\chi}_0$, $\boldsymbol{\chi}_{0\mathbf{q}=0}$ terms in the DMFT BSE with the help of Eqs. (D12) and (D13) and get

$$\boldsymbol{\chi}_{\mathbf{q}=0\pm} = \left[\Gamma + \boldsymbol{\chi}^{-1}_{0\mathbf{q}=0\pm}\right]^{-1}$$

$$= \left[\begin{pmatrix}\boldsymbol{\chi}_s & \boldsymbol{\chi}_{sc}\\ \boldsymbol{\chi}_{cs} & \boldsymbol{\chi}_c\end{pmatrix}^{-1} - \begin{pmatrix}\boldsymbol{\chi}_0 & \overline{\boldsymbol{\chi}}_0\\ \overline{\boldsymbol{\chi}}_0 & \boldsymbol{\chi}_0\end{pmatrix}^{-1}\right.$$

$$\left. + \begin{pmatrix}\boldsymbol{\chi}^{AA}_{0\mathbf{q}=0} \pm \boldsymbol{\chi}^{AB}_{0\mathbf{q}=0} & \overline{\boldsymbol{\chi}}^{AA}_{0\mathbf{q}=0} \mp \overline{\boldsymbol{\chi}}^{AB}_{0\mathbf{q}=0}\\ \overline{\boldsymbol{\chi}}^{AA}_{0\mathbf{q}=0} \pm \overline{\boldsymbol{\chi}}^{AB}_{0\mathbf{q}=0} & \boldsymbol{\chi}^{AA}_{0\mathbf{q}=0} \mp \boldsymbol{\chi}^{AB}_{0\mathbf{q}=0}\end{pmatrix}^{-1}\right]^{-1}$$

$$= \left[\begin{pmatrix}\boldsymbol{\chi}_s & \boldsymbol{\chi}_{sc}\\ \boldsymbol{\chi}_{cs} & \boldsymbol{\chi}_c\end{pmatrix}^{-1} \pm \frac{t^2}{\beta}\begin{pmatrix}\mathbb{1} & 0\\ 0 & -\mathbb{1}\end{pmatrix}\right]^{-1}. \tag{D14}$$

APPENDIX E: BETHE LATTICE: INTERACTION EXPANSION OF THE LOCAL SUSCEPTIBILITY IN A MAGNETIC FIELD

To get an intuitive understanding of the different effects that the magnetic field has on the local generalized susceptibility in weak and strong coupling, we consider an expansion of the local generalized susceptibility in the Bethe lattice in terms of the interaction U.

1. Lowest order ($U = 0$)

In the noninteracting $U = 0$ case, or in the lowest order, the local generalized susceptibility $\boldsymbol{\chi}$ of the Bethe lattice is given by the bare local "bubble" $\boldsymbol{\chi}^{\alpha\alpha(0)}_{0\sigma\sigma} = -\beta(G^0_{\alpha\nu\sigma})^2\delta_{\nu\nu'}$. For a magnetic field h, the local susceptibility in the charge and spin components then reads

$$\boldsymbol{\chi}^{(0)}_0 = \begin{pmatrix}\boldsymbol{\chi}^{\alpha\alpha(0)}_0 & \overline{\boldsymbol{\chi}}^{\alpha\alpha(0)}_0\\ \overline{\boldsymbol{\chi}}^{\alpha\alpha(0)}_0 & \boldsymbol{\chi}^{\alpha\alpha(0)}_0\end{pmatrix}. \tag{E1}$$

When h is staggered (antiferromagnetic with $h_A = -h_B$), the Green's function in the Bethe lattice becomes

$$G^0_{\alpha\nu\sigma} = g^0_\nu\zeta_{\bar{\alpha}\nu\sigma} = g^0_\nu(\mathrm{i}\nu + \mu - \mathrm{sgn}(\sigma)h_\alpha), \tag{E2}$$

with

$$g^0_\nu = \frac{1}{(\mathrm{i}\nu+\mu+h)(\mathrm{i}\nu+\mu-h)\left(1-t^2 g^0_\nu\right)}$$

$$= \frac{1}{2t^2}(\pm)\sqrt{\frac{1}{4t^4} - \frac{1}{t^2(\mathrm{i}\nu+\mu+h)(\mathrm{i}\nu+\mu-h)}}, \tag{E3}$$

where $(\pm)$ has to be chosen such that the Green's function obeys the correct asymptotics for $\nu\to\pm\infty$. The "bubble" reads

$$\boldsymbol{\chi} \overset{U=0}{=} \boldsymbol{\chi}^{(0)}_0$$

$$= \beta\delta_{\nu\nu'}\left(g^0_\nu\right)^2\begin{pmatrix}-(\mathrm{i}\nu+\mu)^2-h^2 & 2h(\mathrm{i}\nu+\mu)\\ 2h(\mathrm{i}\nu+\mu) & -(\mathrm{i}\nu+\mu)^2-h^2\end{pmatrix}. \tag{E4}$$

For half filling ($\mu = 0$), the eigenvalues of $\boldsymbol{\chi}^{(0)}_0$ are

$$\lambda_\pm = \beta\left(g^0_\nu\right)^2(\nu^2 - h^2 \pm 2\mathrm{i}\nu h) \tag{E5}$$

displaying a "fountain"-like structure when plotting their real and imaginary parts for finite magnetic field h, similar to panel (c) of Fig. 5. Here, Eq. (E4) clearly shows the suppressive effect $\propto(\nu^2 - h^2)$ of the magnetic field h on the charge and spin susceptibilities.

2. First order in U

The first-order corrections in U to the local generalized charge susceptibility are displayed in Fig. 9, reading

$$\boldsymbol{\chi}^{(1)}_{0\sigma\sigma} = -2U\beta\delta_{\nu\nu'}\left(G^0_{\nu\sigma}\right)^3\left(\frac{1}{\beta}\sum_{\nu_1}\mathrm{e}^{\mathrm{i}\nu 0^+}G^0_{\nu_1-\sigma}\right), \tag{E6}$$

$$\boldsymbol{\chi}^{(1)}_{\sigma-\sigma} = -U\left(G^0_{\nu\sigma}\right)^2\left(G^0_{\nu'-\sigma}\right)^2. \tag{E7}$$

The former expression in Eq. (E7) corresponds to the first self-energy correction of $\boldsymbol{\chi}_0$ and the latter in Eq. (E7) to the first vertex correction, namely, the bare vertex. At half filling and zero magnetic field, the first self-energy correction is compensated by the chemical potential $\mu = U/2$ and the vertex correction yields a negative contribution, which for

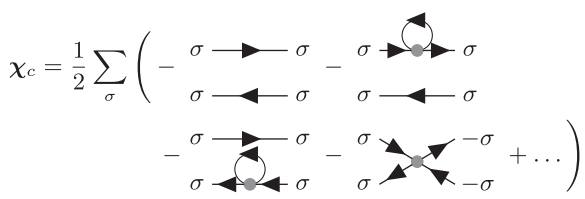


FIG. 9. Diagrammatic representation of the interaction expanded local charge susceptibility, where $G^0_{\nu\sigma} =$ ⟶ and $U =$ ✱.

larger values of U can yield negative eigenvalues in the local charge susceptibility:

$$\boldsymbol{\chi}_c^{(1)} = \frac{1}{2}\sum_{\sigma}\left(\boldsymbol{\chi}_{0\sigma\sigma}^{(0)} + \boldsymbol{\chi}_{0\sigma\sigma}^{(1)} + \boldsymbol{\chi}_{\sigma-\sigma}^{(1)}\right) \tag{E8}$$

(although in lowest order the physical charge response then becomes negative as well).

It is then instructive to consider the change of the different contributions to $\chi_c^{(1)} = (1/\beta^2)\sum_{\nu\nu'}\boldsymbol{\chi}_c^{(1)}$ when turning on a staggered magnetic field h: (1) $\chi_0^{(0)} = (1/2\beta^2)\sum_{\nu\nu'\sigma}\boldsymbol{\chi}_{0\sigma\sigma}^{(0)}$ remains positive and becomes suppressed, as discussed in the preceding section; (2) $\chi_0^{(1)} = (1/2\beta^2)\sum_{\nu\nu'\sigma}\boldsymbol{\chi}_{0\sigma\sigma}^{(1)}$ will become nonzero and negative, further suppressing $\chi_c^{(1)}$; and (3) $(1/2)\sum_{\sigma}\chi_{\sigma-\sigma}^{(1)} = (1/2\beta^2)\sum_{\nu\nu'\sigma}\boldsymbol{\chi}_{\sigma-\sigma}^{(1)}$ becomes *less* negative, since $(G_{\nu\sigma}^0)^2$ is getting smaller. The overall change of the charge response in first order with increasing U thus depends on the delicate balance between the suppressive term of $\chi_0^{(1)}$ and the effectively *enhancing* term of the vertex in $\chi_c^{(1)}$. For small values of the interaction, the suppressive effect of $\chi_0^{(0)}$ will generally dominate the behavior of χ_c. With increasing U at $h = 0$, the vertex contributions dominate and lead to negative eigenvalues in the charge susceptibility also for higher order in U. For finite magnetic field $h > 0$, the balance between the suppressive and enhancing contributions depending on the lattice and magnetic field in $G_{\nu\sigma}^0$ then determines the overall behavior of the local charge response at strong coupling. The delicate balance can also be made responsible for the overall suppressive effect of h in the RPA approximation; there, the self-energy corrections are not treated on equal footing with the vertex corrections (not in the same order of U), not allowing for negative eigenvalues and tipping the balance to the suppressive side.

On the other hand, in DMFT, the correct treatment of interaction diagrams order per order in the Monte Carlo sampling of the auxiliary AIM can tip the balance to the vertex corrections, and the magnetic field can lead to an enhancement of the local charge response in the regime of the Heisenberg antiferromagnet.

APPENDIX F: CHARGE RESPONSE IN THE ATOMIC LIMIT AT *ph* SYMMETRY

For the atomic limit of the Hubbard model (AL) in a magnetic field h at *ph* symmetry $\mu = U/2$,

$$H = -\frac{U}{2}(\hat{n}_\uparrow + \hat{n}_\downarrow) - h(\hat{n}_\uparrow - \hat{n}_\downarrow) + U\hat{n}_\uparrow\hat{n}_\downarrow, \tag{F1}$$

the local charge response χ_c becomes always suppressed for $|h| > 0$, in comparison with $h = 0$:

$$\chi_c = \frac{\beta}{e^{\frac{\beta U}{2}}\cosh(\beta h) + 1}, \tag{F2}$$

since $\cosh(\beta h) > 1$ for $|h| > 0$. This is in contrast to the strong-coupling limit of the Heisenberg AF in DMFT, where χ_c becomes enhanced in the AF phase (as discussed in Sec. III B). However,, the eigenspectra of the local generalized susceptibilities $\boldsymbol{\chi}$ look qualitatively similar between the AL and the Heisenberg AF: Both show similar eigenvalues—including negative ones—and have similar eigenvectors. This difference in the charge response χ_c illustrates that negative eigenvalues are a necessary requirement—since they stem from the dominant negative vertex contributions—allowing for the local enhancement of the charge response in a magnetic field. However, they alone may not be sufficient. The behavior of the physical response, suppressive or repulsive, still depends on the overall balance between the bubble $\boldsymbol{\chi}_0$ and the vertex contributions to χ_c.

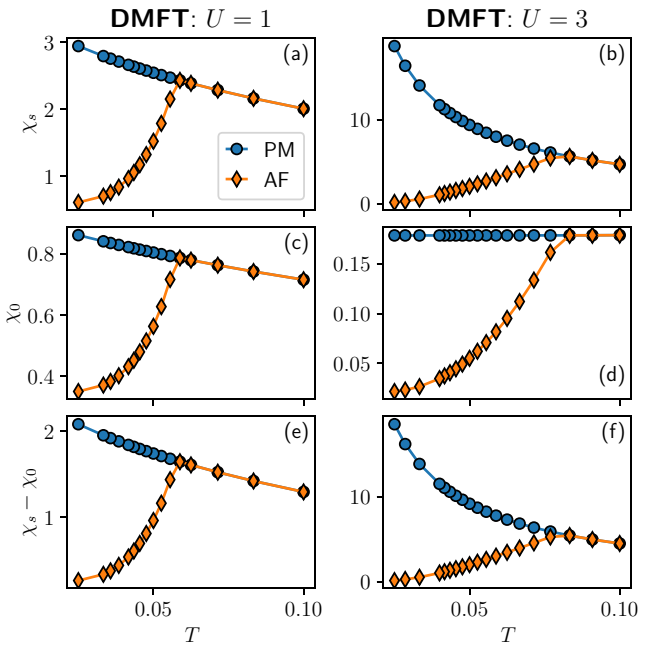


FIG. 10. Comparision of the local spin response χ_s and of its different diagrammatic contributions as a function of temperature T in our AF (orange diamonds) and PM (blue circles) DMFT calculations for weak coupling $U = 1$ (left column) and strong coupling $U = 3$. Top row: Local spin response χ_s. Middle row: Bubble contribution χ_0 to χ_s. Bottom row: The difference between the bubble contribution χ_0 and χ_s, corresponding to the vertex corrections.

APPENDIX G: LOCAL SPIN RESPONSE

In contrast to the local charge response χ_c (see Sec. III B), the local spin response $\chi_s = (1/\beta^2)\sum_{\nu\nu'}\boldsymbol{\chi}_s$, calculated in DMFT, decreases in the weak-coupling Slater AF and in the strong-coupling Heisenberg AF regime with respect to the PM solution. The qualitative similar effect of the AF order onto $\chi_s(T)$ for two representative values for weak and strong coupling, $U = 1$ and $U = 3$, respectively, can be observed in the top row of Fig. 10, where we compare χ_s, similar to χ_c in Fig. 4. Since the bubble contribution χ_0 to χ_s (middle row) is the same as for χ_c, the difference in the behavior stems from the vertex contributions $\chi_{\text{vert}} = \chi_s - \chi_0$ (bottom row). In contrast to the case of χ_c, for χ_s the vertex corrections χ_{vert} have a positive value and decrease in the AF phase with respect to the PM solution, showing a similar suppressive behavior as χ_0.

This different behavior can be already understood at the level of the first-order vertex correction $\boldsymbol{\chi}_{\sigma-\sigma}^{(1)}$ (see Appendix E), which enters χ_s with the opposite sign in

comparison to χ_c [cf. Eq. (12)]. At the same time, additional negative real eigenvalues of $\boldsymbol{\chi}$ in the AF Heisenberg regime, stemming from spin-dominated vertex divergence lines, have an additional suppressive effect on χ_s. Thus, they further contribute to the suppression of χ_s in the AF strong-coupling regime.

[1] H. von Löhneysen, A. Rosch, M. Vojta, and P. Wölfle, Fermi-liquid instabilities at magnetic quantum phase transitions, Rev. Mod. Phys. **79**, 1015 (2007).

[2] M. Brando, D. Belitz, F. M. Grosche, and T. R. Kirkpatrick, Metallic quantum ferromagnets, Rev. Mod. Phys. **88**, 025006 (2016).

[3] T. Schäfer, A. A. Katanin, K. Held, and A. Toschi, Interplay of correlations and Kohn anomalies in three dimensions: Quantum criticality with a twist, Phys. Rev. Lett. **119**, 046402 (2017).

[4] S. Adler, D. R. Fus, M. O. Malcolms, A. Vock, K. Held, A. A. Katanin, T. Schäfer, and A. Toschi, Magnetic quantum criticality dynamical mean-field perspective, arXiv:2409.04308 [cond-mat.str-el].

[5] T. Timusk and B. Statt, The pseudogap in high-temperature superconductors: An experimental survey, Rep. Prog. Phys. **62**, 61 (1999).

[6] O. Gunnarsson, T. Schäfer, J. P. F. LeBlanc, E. Gull, J. Merino, G. Sangiovanni, G. Rohringer, and A. Toschi, Fluctuation diagnostics of the electron self-energy: Origin of the pseudogap physics, Phys. Rev. Lett. **114**, 236402 (2015).

[7] P. Worm, M. Reitner, K. Held, and A. Toschi, Fermi and Luttinger arcs: Two concepts, realized on one surface, Phys. Rev. Lett. **133**, 166501 (2024).

[8] J. Krsnik and K. Held, Local correlations necessitate waterfalls as a connection between quasiparticle band and developing Hubbard bands, Nat. Commun. **16**, 255 (2025).

[9] T. Schäfer, G. Rohringer, O. Gunnarsson, S. Ciuchi, G. Sangiovanni, and A. Toschi, Divergent precursors of the Mott-Hubbard transition at the two-particle level, Phys. Rev. Lett. **110**, 246405 (2013).

[10] E. Kozik, M. Ferrero, and A. Georges, Nonexistence of the Luttinger-Ward functional and misleading convergence of skeleton diagrammatic series for Hubbard-like models, Phys. Rev. Lett. **114**, 156402 (2015).

[11] A. Stan, P. Romaniello, S. Rigamonti, L. Reining, and J. A. Berger, Unphysical and physical solutions in many-body theories: From weak to strong correlation, New J. Phys. **17**, 093045 (2015).

[12] O. Gunnarsson, T. Schäfer, J. P. F. LeBlanc, J. Merino, G. Sangiovanni, G. Rohringer, and A. Toschi, Parquet decomposition calculations of the electronic self-energy, Phys. Rev. B **93**, 245102 (2016).

[13] O. Gunnarsson, G. Rohringer, T. Schäfer, G. Sangiovanni, and A. Toschi, Breakdown of traditional many-body theories for correlated electrons, Phys. Rev. Lett. **119**, 056402 (2017).

[14] P. Chalupa, P. Gunacker, T. Schäfer, K. Held, and A. Toschi, Divergences of the irreducible vertex functions in correlated metallic systems: Insights from the Anderson impurity model, Phys. Rev. B **97**, 245136 (2018).

[15] W. Tarantino, B. S. Mendoza, P. Romaniello, J. A. Berger, and L. Reining, Many-body perturbation theory and non-perturbative approaches: Screened interaction as the key ingredient, J. Phys.: Condens. Matter **30**, 135602 (2018).

[16] J. Vučičević, N. Wentzell, M. Ferrero, and O. Parcollet, Practical consequences of the Luttinger-Ward functional multivaluedness for cluster dmft methods, Phys. Rev. B **97**, 125141 (2018).

[17] D. Springer, P. Chalupa, S. Ciuchi, G. Sangiovanni, and A. Toschi, Interplay between local response and vertex divergences in many-fermion systems with on-site attraction, Phys. Rev. B **101**, 155148 (2020).

[18] M. Reitner, L. Crippa, D. R. Fus, J. C. Budich, A. Toschi, and G. Sangiovanni, Protection of correlation-induced phase instabilities by exceptional susceptibilities, Phys. Rev. Res. **6**, L022031 (2024).

[19] H. Eßl, M. Reitner, G. Sangiovanni, and A. Toschi, General Shiba mapping for on-site four-point correlation functions, Phys. Rev. Res. **6**, 033061 (2024).

[20] M. Reitner, P. Chalupa, L. Del Re, D. Springer, S. Ciuchi, G. Sangiovanni, and A. Toschi, Attractive effect of a strong electronic repulsion: The physics of vertex divergences, Phys. Rev. Lett. **125**, 196403 (2020).

[21] P. Chalupa, T. Schäfer, M. Reitner, D. Springer, S. Andergassen, and A. Toschi, Fingerprints of the local moment formation and its Kondo screening in the generalized susceptibilities of many-electron problems, Phys. Rev. Lett. **126**, 056403 (2021).

[22] T. B. Mazitov and A. A. Katanin, Local magnetic moment formation and Kondo screening in the half-filled single-band Hubbard model, Phys. Rev. B **105**, L081111 (2022).

[23] T. B. Mazitov and A. A. Katanin, Effect of local magnetic moments on spectral properties and resistivity near interaction- and doping-induced Mott transitions, Phys. Rev. B **106**, 205148 (2022).

[24] S. Adler, F. Krien, P. Chalupa-Gantner, G. Sangiovanni, and A. Toschi, Non-perturbative intertwining between spin and charge correlations: A "smoking gun" single-boson-exchange result, SciPost Phys. **16**, 054 (2024).

[25] A. Kowalski, M. Reitner, L. Del Re, M. Chatzieleftheriou, A. Amaricci, A. Toschi, L. de' Medici, G. Sangiovanni, and T. Schäfer, Thermodynamic stability at the two-particle level, Phys. Rev. Lett. **133**, 066502 (2024).

[26] T. Schäfer, S. Ciuchi, M. Wallerberger, P. Thunström, O. Gunnarsson, G. Sangiovanni, G. Rohringer, and A. Toschi, Nonperturbative landscape of the Mott-Hubbard transition: Multiple divergence lines around the critical endpoint, Phys. Rev. B **94**, 235108 (2016).

[27] M. Pelz, S. Adler, M. Reitner, and A. Toschi, Highly non-perturbative nature of the Mott metal-insulator transition: Two-particle vertex divergences in the coexistence region, Phys. Rev. B **108**, 155101 (2023).

[28] R. Nourafkan, M. Côté, and A.-M. S. Tremblay, Charge fluctuations in lightly hole-doped cuprates: Effect of vertex corrections, Phys. Rev. B **99**, 035161 (2019).

[29] M. Grilli and C. Castellani, Electron-phonon interactions in the presence of strong correlations, Phys. Rev. B **50**, 16880 (1994).

[30] M. Capone, C. Castellani, and M. Grilli, Electron-phonon interaction in strongly correlated systems, Adv. Condens. Matter Phys. **2010**, 920860 (2010).

[31] M. Grilli, R. Raimondi, C. Castellani, C. Di Castro, and G. Kotliar, Superconductivity, phase separation, and charge-transfer instability in the $U = \infty$ limit of the three-band model of the CuO_2 planes, Phys. Rev. Lett. **67**, 259 (1991).

[32] V. Emery and S. Kivelson, Frustrated electronic phase separation and high-temperature superconductors, Physica C **209**, 597 (1993).

[33] E. Dagotto, J. Riera, Y. C. Chen, A. Moreo, A. Nazarenko, F. Alcaraz, and F. Ortolani, Superconductivity near phase separation in models of correlated electrons, Phys. Rev. B **49**, 3548 (1994).

[34] S. Rohshap, M. K. Ritter, H. Shinaoka, J. von Delft, M. Wallerberger, and A. Kauch, Two-particle calculations with quantics tensor trains: Solving the parquet equations, Phys. Rev. Res. **7**, 023087 (2025).

[35] A. Georges, G. Kotliar, W. Krauth, and M. J. Rozenberg, Dynamical mean-field theory of strongly correlated fermion systems and the limit of infinite dimensions, Rev. Mod. Phys. **68**, 13 (1996).

[36] T. Maier, M. Jarrell, T. Pruschke, and M. H. Hettler, Quantum cluster theories, Rev. Mod. Phys. **77**, 1027 (2005).

[37] G. Sangiovanni, A. Toschi, E. Koch, K. Held, M. Capone, C. Castellani, O. Gunnarsson, S.-K. Mo, J. W. Allen, H.-D. Kim, A. Sekiyama, A. Yamasaki, S. Suga, and P. Metcalf, Static versus dynamical mean-field theory of Mott antiferromagnets, Phys. Rev. B **73**, 205121 (2006).

[38] C. Taranto, G. Sangiovanni, K. Held, M. Capone, A. Georges, and A. Toschi, Signature of antiferromagnetic long-range order in the optical spectrum of strongly correlated electron systems, Phys. Rev. B **85**, 085124 (2012).

[39] A. Toschi, M. Capone, and C. Castellani, Energetic balance of the superconducting transition across the BCS—Bose Einstein crossover in the attractive Hubbard model, Phys. Rev. B **72**, 235118 (2005).

[40] G. Rohringer, H. Hafermann, A. Toschi, A. A. Katanin, A. E. Antipov, M. I. Katsnelson, A. I. Lichtenstein, A. N. Rubtsov, and K. Held, Diagrammatic routes to nonlocal correlations beyond dynamical mean field theory, Rev. Mod. Phys. **90**, 025003 (2018).

[41] Y. M. Vilk and A.-M. S. Tremblay, Non-perturbative many-body approach to the Hubbard model and single-particle pseudogap, J. Phys. I France **7**, 1309 (1997).

[42] L. Del Re and A. Toschi, Dynamical vertex approximation for many-electron systems with spontaneously broken SU(2) symmetry, Phys. Rev. B **104**, 085120 (2021).

[43] L. Del Re, Dirac points and topological phases in correlated altermagnets, arXiv:2408.14288 [cond-mat.str-el].

[44] N. Bickers, Self-consistent many-body theory for condensed matter systems, in *Theoretical Methods for Strongly Correlated Electrons*, edited by D. Sénéchal, A. Tremblay, and C. Bourbonnais (Springer, New York, 2004), pp. 237–296.

[45] S. M. Girvin and K. Yang, *Modern Condensed Matter Physics* (Cambridge University Press, Cambridge, 2019), Chap. 7.5.

[46] P. M. Bonetti and W. Metzner, Su(2) gauge theory of the pseudogap phase in the two-dimensional Hubbard model, Phys. Rev. B **106**, 205152 (2022).

[47] I. A. Goremykin and A. A. Katanin, Antiferromagnetic and spin spiral correlations in the doped two-dimensional Hubbard model: Gauge symmetry, Ward identities, and dynamical mean-field theory analysis, Phys. Rev. B **110**, 085153 (2024).

[48] E. Gull, A. J. Millis, A. I. Lichtenstein, A. N. Rubtsov, M. Troyer, and P. Werner, Continuous-time Monte Carlo methods for quantum impurity models, Rev. Mod. Phys. **83**, 349 (2011).

[49] M. Wallerberger, A. Hausoel, P. Gunacker, A. Kowalski, N. Parragh, F. Goth, K. Held, and G. Sangiovanni, W2dynamics: Local one- and two-particle quantities from dynamical mean field theory, Comput. Phys. Commun. **235**, 388 (2019).

[50] A. V. Chubukov and D. M. Frenkel, Renormalized perturbation theory of magnetic instabilities in the two-dimensional Hubbard model at small doping, Phys. Rev. B **46**, 11884 (1992).

[51] G. Rohringer, A. Valli, and A. Toschi, Local electronic correlation at the two-particle level, Phys. Rev. B **86**, 125114 (2012).

[52] F. B. Kugler, S.-S. B. Lee, and J. von Delft, Multipoint correlation functions: Spectral representation and numerical evaluation, Phys. Rev. X **11**, 041006 (2021).

[53] C. Watzenböck, M. Fellinger, K. Held, and A. Toschi, Long-term memory magnetic correlations in the Hubbard model: A dynamical mean-field theory analysis, SciPost Phys. **12**, 184 (2022).

[54] W. Metzner and D. Vollhardt, Correlated lattice fermions in $d = \infty$ dimensions, Phys. Rev. Lett. **62**, 324 (1989).

[55] A. Lee, Centrohermitian and skew-centrohermitian matrices, Linear Algebra Appl. **29**, 205 (1980), special Volume Dedicated to Alson S. Householder.

[56] J. C. Ward, An identity in quantum electrodynamics, Phys. Rev. **78**, 182 (1950).

[57] F. Krien, E. G. C. P. van Loon, H. Hafermann, J. Otsuki, M. I. Katsnelson, and A. I. Lichtenstein, Conservation in two-particle self-consistent extensions of dynamical mean-field theory, Phys. Rev. B **96**, 075155 (2017).

[58] A. J. Kim and V. Sacksteder, Multivaluedness of the Luttinger-Ward functional in the fermionic and bosonic system with replicas, Phys. Rev. B **101**, 115146 (2020).

[59] H. Eßl, M. Reitner, E. Kozik, and A. Toschi, How to stay on the physical branch in self-consistent many-electron approaches, arXiv:2502.01420 [cond-mat.str-el].

[60] N. Blümer, Mott-Hubbard metal-insulator transition and optical conductivity in high dimensions, Ph.D. thesis, Universität Mainz, 2002.

[61] J. Kuneš, Efficient treatment of two-particle vertices in dynamical mean-field theory, Phys. Rev. B **83**, 085102 (2011).

[62] P. G. J. van Dongen, Extended Hubbard model at weak coupling, Phys. Rev. B **50**, 14016 (1994).

[63] A. Toschi, M. Capone, M. Ortolani, P. Calvani, S. Lupi, and C. Castellani, Temperature dependence of the optical spectral weight in the cuprates: Role of electron correlations, Phys. Rev. Lett. **95**, 097002 (2005).

[64] L. Del Re and G. Rohringer, Fluctuations analysis of spin susceptibility: Néel ordering revisited in dynamical mean field theory, Phys. Rev. B **104**, 235128 (2021).

[65] E. G. C. P. van Loon, Second-order phase transitions and divergent linear response in dynamical mean-field theory, Phys. Rev. B **109**, L241110 (2024).

[66] E. G. C. P. van Loon, Two-particle correlations and the metal-insulator transition: Iterated perturbation theory revisited, Phys. Rev. B **105**, 245104 (2022).

[67] E. Moghadas, M. Reitner, T. Wehling, G. Sangiovanni, S. Ciuchi, and A. Toschi, Effective enhancement of the electron-phonon coupling driven by nonperturbative electronic density fluctuations, arXiv:2503.12113 [cond-mat.str-el].

[68] V. Janiš and V. Pokorný, Critical metal-insulator transition and divergence in a two-particle irreducible vertex in disordered and interacting electron systems, Phys. Rev. B **90**, 045143 (2014).

[69] R. Rossi and F. Werner, Skeleton series and multivaluedness of the self-energy functional in zero space-time dimensions, J. Phys. A: Math. Theor. **48**, 485202 (2015).

[70] R. Rossi, F. Werner, N. Prokof'ev, and B. Svistunov, Shifted-action expansion and applicability of dressed diagrammatic schemes, Phys. Rev. B **93**, 161102(R) (2016).

[71] E. G. C. P. van Loon, F. Krien, and A. A. Katanin, Bethe-salpeter equation at the critical end point of the Mott transition, Phys. Rev. Lett. **125**, 136402 (2020).

[72] A. K. Arzhnikov and A. G. Groshev, Effect of thermal fluctuations on magnetic phase separation and on the parameters of spin-spiral waves, JETP Lett. **94**, 703 (2012).

[73] C. Lenihan, A. J. Kim, F. Šimkovic, and E. Kozik, Evaluating second-order phase transitions with diagrammatic Monte Carlo: Néel transition in the doped three-dimensional Hubbard model, Phys. Rev. Lett. **129**, 107202 (2022).

[74] L. Rampon, F. Šimkovic, and M. Ferrero, Magnetic phase diagram of the three-dimensional doped Hubbard model, Phys. Rev. Lett. **134**, 066502 (2025).

[75] C. Castellani, C. Di Castro, and M. Grilli, Singular quasiparticle scattering in the proximity of charge instabilities, Phys. Rev. Lett. **75**, 4650 (1995).

[76] S. Sorella, The phase diagram of the Hubbard model by variational auxiliary field quantum Monte Carlo, arXiv:2101.07045 [cond-mat.str-el].

[77] A. Toschi, A. A. Katanin, and K. Held, Dynamical vertex approximation: A step beyond dynamical mean-field theory, Phys. Rev. B **75**, 045118 (2007).

[78] C. Taranto, S. Andergassen, J. Bauer, K. Held, A. Katanin, W. Metzner, G. Rohringer, and A. Toschi, From infinite to two dimensions through the functional renormalization group, Phys. Rev. Lett. **112**, 196402 (2014).

[79] N. Wentzell, C. Taranto, A. Katanin, A. Toschi, and S. Andergassen, Correlated starting points for the functional renormalization group, Phys. Rev. B **91**, 045120 (2015).

[80] L. Del Re, Two-particle self-consistent approach for broken symmetry phases, SciPost Phys. **18**, 077 (2025).

[81] M. Qin, T. Schäfer, S. Andergassen, P. Corboz, and E. Gull, The Hubbard model: A computational perspective, Annu. Rev. Condens. Matter Phys. **13**, 275 (2022).

[82] N. D. Mermin and H. Wagner, Absence of ferromagnetism or antiferromagnetism in one- or two-dimensional isotropic Heisenberg models, Phys. Rev. Lett. **17**, 1133 (1966).

[83] T. Baier, E. Bick, and C. Wetterich, Temperature dependence of antiferromagnetic order in the Hubbard model, Phys. Rev. B **70**, 125111 (2004).

[84] S. Jenkins, L. Rózsa, U. Atxitia, R. F. L. Evans, K. S. Novoselov, and E. J. G. Santos, Breaking through the Mermin-Wagner limit in 2D van der Waals magnets, Nat. Commun. **13**, 6917 (2022).

[85] A.-M. Daré, Y. M. Vilk, and A. M. S. Tremblay, Crossover from two- to three-dimensional critical behavior for nearly antiferromagnetic itinerant electrons, Phys. Rev. B **53**, 14236 (1996).

[86] A.-M. S. Tremblay, Two-particle-self-consistent approach for the Hubbard model, in *Strongly Correlated Systems*, edited by A. Avella and F. Mancini (Springer, Berlin, 2011), pp. 409–453.

[87] T. Schäfer, F. Geles, D. Rost, G. Rohringer, E. Arrigoni, K. Held, N. Blümer, M. Aichhorn, and A. Toschi, Fate of the false Mott-Hubbard transition in two dimensions, Phys. Rev. B **91**, 125109 (2015).

[88] T. Schäfer *et al.*, Tracking the footprints of spin fluctuations: A multimethod, multimessenger study of the two-dimensional Hubbard model, Phys. Rev. X **11**, 011058 (2021).

[89] E. Gull, P. Werner, X. Wang, M. Troyer, and A. J. Millis, Local order and the gapped phase of the Hubbard model: A plaquette dynamical mean-field investigation, Europhys. Lett. **84**, 37009 (2008).

[90] M. Reitner, L. Del Re, M. Capone, and A. Toschi, Dataset for: "NonPerturbative feats in the physics of correlated antiferromagnets", 2025, doi:10.48436/6wz77-3sz27

[91] R. D. Hill and S. R. Waters, On $\varkappa$-real and $\varkappa$-Hermitian matrices, Linear Algebra Appl. **169**, 17 (1992).

[92] L. Del Re and M. Capone, Selective insulators and anomalous responses in three-component fermionic gases with broken SU(3) symmetry, Phys. Rev. A **98**, 063628 (2018).